TABLE IV. Mutation Spectra of Mouse Lymphoma *Tk* Mutants from the AZT-Treated Culture and Untreated Independent Control Cultures

Source of mutants	Clone size (No.)	Intragenic mutation	Deletion	Chromosome loss	Recombination	Chromosome duplication	Mosaic/ Complex
Mutants from AZT-treated culture[a]	LC (55)	14 (25%)	12 (22%)	1 (2%)	16 (29%)	6 (11%)	6 (11%)
	SC (95)	0 (0%)	39 (41%)	2 (2%)	32 (34%)	10 (11%)	12 (13%)
	Total[b] (150)	13 (9%)	51 (34%)	3 (2%)	48 (32%)	16 (11%)	18 (12%)
Spontaneous mutants	LC (36)	21 (58%)	0 (0%)	0 (0%)	9 (25%)	5 (14%)	1 (3%)
	SC (33)	1 (3%)	9 (27%)	1 (3%)	9 (27%)	7 (21%)	6 (18%)
	Total[b] (69)	25 (36%)	8 (11%)	1 (1%)	18 (26%)	12 (17%)	6 (9%)

LC: large colony; SC: small colony.

[a]The culture that the analyzed mutants were isolated from was treated with 1 mg/ml (3,742 μM) AZT for 24 hr.

[b]Total is the weighted sum of the number of LC and SC mutants considering the proportion difference of LC and SC mutants between the selected mutants and mutants in the original culture (the proportion of SC mutants was 65 and 40% in the AZT-treated culture and untreated control, respectively).

The SC mutants contained more deletions and fewer intragenic mutations than did the LC mutants.

DISCUSSION

AZT, a synthetic thymidine analogue developed to treat AIDS, has been used widely to treat and prevent HIV infection since its approval by the US FDA in 1987. Its therapeutic effect is due to the inhibition of HIV reverse transcriptase as well as the termination of proviral DNA synthesis. However, AZT also can incorporate into the mammalian cell nuclear DNA and the incorporation is closely correlated with its genotoxicity [Vazquez-Padua et al., 1990; Sussman et al., 1999; Meng et al., 2000b]. Molecular analysis indicates that the majority of AZT-induced mutations in autosomal genes are due to LOH [Meng et al., 2000a,b; Von Tungeln et al., 2002]. LOH is an important mechanism for the functional loss of critical genes, such as tumor suppressor genes, and it is the most common mutational mechanism in the etiology of human cancer [Lasko and Cavenee, 1991; Wijnhoven et al., 2001; Thiagalingam et al., 2002]. Our data are consistent with those previous findings. At a dose of 1 mg/ml (3,742 μM), 91% of AZT-induced mutants showed LOH at the *Tk* locus while *Tk* LOH was detected in only 64% of spontaneous mutants.

AZT is a thymidine analogue; therefore, using the *Tk* gene as the mutational target raises the issue that the increase in MF might be due to selection of pre-existing mutants rather than induction of new mutants. AZT is activated by a series of phosphorylation reactions to AZT triphosphate to elicit its therapeutic effects as well as its toxicity. The first step of the activation (AZT → AZT monophosphate) is catalyzed by thymidine kinase [Veal and Back, 1995]. Because AZT cannot be activated without a functional Tk, this raises the possibility that the pre-existing $Tk^{-/-}$ mutants may avoid the toxicity of AZT. As a consequence, the pre-existing mutants may gain a growth advantage over the $Tk^{+/-}$ cells and the *Tk* MF will be increased by this differential cytotoxicity. In studies using B6C3F1/$Tk^{+/-}$ mice, Von Tungeln et al. [2002] and Mit-

telstaedt et al. [2004] found that the percentage of mutants showing LOH at the *Tk* locus and also the LOH pattern differed between the mutants from the AZT-treated animals and the untreated control animals. Their results indicated that de novo mutation induction rather than pre-existing mutant selection played the major role in the MF elevation. Our study, by further clarifying the AZT-induced mutation spectrum in mouse lymphoma cells, confirms this conclusion. The mutation spectrum of mutants from the AZT-treated culture was distinct from that of the spontaneous mutants. If the MF increase was primarily due to mutant selection, then the mutation spectra of mutants from AZT-treated culture and untreated control should have been the same.

Mittelstaedt et al. [2004] found a relatively high proportion of discontinuous LOH patterns in the mutants from AZT-treated B6C3F1/$Tk^{+/-}$ mice. Von Tungeln et al. [2007] also found discontinuous LOH patterns in the mutants from neonatal offspring of B6C3F1/$Tk^{+/-}$ mice transplacetally exposed to AZT. Discontinuous LOH is two areas of LOH in a single chromosome interrupted by a section of the chromosome without LOH. *Tk* mutant lymphocytes (20%) isolated from the AZT-treated mice contained discontinuous LOH and no discontinuous LOH was observed in the control [Mittelstaedt et al., 2004]. Discontinuous LOH is thought to result from chromosome instability and it is caused by multiple deletions and/or mitotic recombination events [Turker et al., 1999]. Turker et al. [1999] observed these novel LOH patterns in an $Aprt^{+/-}$ kidney cell line after exposure to hydrogen peroxide. They hypothesized that the discontinuous LOH resulted from oxidative damage. Later Ponomareva et al. [2002] observed this pattern in ionizing radiation-induced *Aprt* mutants from ear and kidney tissues and they suspected that it resulted from genomic instability following mutation. In our study, we found only three out of 150 mutants from the AZT-treated culture had discontinuous LOH. The reason for this difference in discontinuous LOH generation in mouse lymphoma cells and the lymphocytes of $Tk^{+/-}$ mice [Mittelstaedt et al., 2004] is not clear.

Environmental and Molecular Mutagenesis. DOI 10.1002/em

AZT-Induced Deletion   255

LOH is thought to result from either a deletion or a recombination event between homologous alleles during the repair of DNA double-strand breaks (DSBs) [Honma, 2005]. Mutation types are determined not only by the nature of the DNA damage but also by the nature of the DNA repair. Different DNA repair pathways may yield different types of mutation [Pastink et al., 2001]. DSBs are usually induced by ionizing radiation, clastogens, and endogenously generated reactive oxygen species. Their repair is important to the maintenance of genomic integrity, which is essential for cellular survival in mammals [Khanna and Jackson, 2001]. In mammalian cells, there are two main pathways for the repair of DNA DSBs: nonhomologous end-joining (NHEJ) and homologous recombination (HR), with NEHJ as the major repair pathway [Jackson, 2002; Helleday, 2003; Honma et al., 2003]. NHEJ repairs DSBs by processing the two broken DNA ends first, followed by joining and ligation. Since this repair mechanism occurs in a nonconservative manner, it often results in deletions. Although HR is conservative and usually error-free, it may result in recessive mutation when the template allele has a mutation. Both NEHJ and HR result in LOH [Rathmell and Chu, 1998]. In addition, there is evidence indicating that illegitimate (nonhomologous) recombination is also an important pathway for DSB repair in mammalian cells and significantly contributes to the generation of LOH in p53-mutant cells [Honma et al., 1997; Sargent et al., 1997]. Because the L5178Y mouse lymphoma cell line has two mutant p53 alleles [Storer et al., 1997; Clark et al., 1998], this mechanism may contribute to the LOH induced by AZT in these cells.

LOH has been studied in various systems, but very few studies further investigated the nature of the LOH. Most previous studies provided data from which the authors speculated as to the actual mutation events [Turker et al., 1999]. Without gene dosage analysis and cytogenetic analysis, such predictions may not be correct. Southern blot analysis has been used to detect allele polymorphism and gene dosage [Applegate et al., 1990; Clive et al., 1990; Meng et al., 2002]. However, this method has several disadvantages. It is time consuming, requires a relatively large amount of DNA, and cannot measure gene dosage with precision [Joseph et al., 1993]. Cytogenetic analysis of mutants is also informative [Hozier et al., 1981; Moore et al., 1985; Blazak et al., 1989; Zhang et al., 1996]. Wijnhoven et al. [1998] used a dual-colored FISH-analysis to measure the gene dosage in the Aprt locus. However, because cytogenetic analysis is also time consuming and technically demanding, the number of mutants that can be reasonably analyzed is somewhat limited. For this study, we developed a Real-Time PCR method to detect Tk gene dosage rapidly and with satisfactory precision. We used an unrelated gene (H-2K) that resides on chromosome 17 as an endogenous reference [Honma et al., 2001]. In the L5178Y/Tk$^{+/-}$ 3.7.2C mouse lymphoma cell line, chromo-

some 17 is cytogenetically stable and diploid [Sawyer et al., 2005].

A higher proportion of deletions (34% vs. 11%) and a lower proportion of intragenic mutations (9% vs. 36%) were observed in the mutants from the AZT-treated culture compared with the spontaneous mutants; while the proportion of recombination events increased only slightly in the mutants from the AZT-treated culture compared with the spontaneous mutants (32% vs. 26%). These data indicate that AZT mainly induces large-scale DNA damage in mouse lymphoma cells and a large number of induced mutations are deletions. The greatly increased frequency of deletions may result from insufficient HR repair, NEHJ repair, or illegitimate recombination [Sargent et al., 1997; Honma et al., 2003].

The DSBs induced by AZT are a severe form of DNA damage, and normal cells with unrepaired DSBs usually can not survive. DSBs lead to cell death through p53-dependent pathways [Khanna and Jackson, 2001; Honma, 2005]. Honma et al. [2000, 2005] conducted extensive research on the effects of p53 status on mutation manifestation in human lymphoblastoid cell lines and found that a higher frequency of large deletions and chromosome changes were induced in p53-mutant cell lines. Our data are consistent with these findings. In the L5178Y/Tk$^{+/-}$ - 3.7.2C mouse lymphoma cell line, both p53 alleles are mutant [Storer et al., 1997; Clark et al., 1998], and this may explain why a large number of mutants with large deletions survived.

In summary, the genotoxicity of AZT has been characterized in L5178Y/Tk$^{+/-}$ mouse lymphoma cells. Taking advantage of a Real-Time PCR technique, our study is the first to clarify the mutation spectrum induced by AZT. A large number of the mutants from AZT-treated culture result from deletion.

ACKNOWLEDGMENTS

REFERENCES

Adams WT, Skopek TR. 1987. Statistical test for the comparison of samples from mutational spectra. J Mol Biol 194:391–396.

Agarwal RP, Olivero OA. 1997. Genotoxicity and mitochondria damage in human lymphocytic cells chronically exposed to 3'-azido-3'-dideoxythymidine. Mutat Res 390:223–231.

Applegate ML, Moore MM, Broder CB, Burrell A, Juhn G, Kasweck KL, Lin PF, Wadhams A, Hozier JC. 1990. Molecular dissection of mutations at the heterozygous thymidine kinase locus in mouse lymphoma cells. Proc Natl Acad Sci USA 87:51–55.

Ayers KM, Clive D, Tucker WE, Hajian G, Miranda PD. 1996. Nonclinical toxicology studies with zidovudine: Genetic toxicity tests and carcinogenicity bioassays in mice and rats. Fundam Appl Toxicol 32:148–158.

Ayers KM, Torrey CE, Reynolds DJ. 1997. A transplacental carcinogenicity bioassay in CD-1 mice with zidovudine. Fundam Appl Toxicol 38:195–198.

Blazak WF, Los FJ, Rudd CJ, Caspary WJ. 1989. Chromosome analysis of small and large L5178Y mouse lymphoma cell colonies: Comparison of trifluorothymidine-resistant and unselected cell colonies from mutagen-treated and control cultures. Mutat Res 224:197–208.

Cariello NF. 1994. Software for the analysis of mutations at the human Hprt gene. Mutat Res 312:173–185.

Chen T, Moore MM. 2004.Screening for chemical mutagens using the mouse lymphoma assay. In: Yan Z,Caldwell GW, editors. Optimization in Drug Discovery: In-Vitro Methods. Totowa, NJ: Humana Press. pp 337–352.

Clark LS, Hart DW, Vojta PJ, Harrington-Brock K, Barrett JC, Moore MM, Tindall KR. 1998. Identification and chromosomal assignment of two heterozygous mutations in the Trp53 gene in L5178Y Tk$^{+/-}$ 3.7.2 C mouse lymphoma cells. Mutagen 13:427–434.

Clive D, Glover P, Applegate M, Hozier J. 1990. Molecular aspects of chemical mutagenesis in L5178Y/Tk$^{+/-}$ mouse lymphoma cells. Mutagen 5:191–197.

Connor EM, Sperling RS, Gelber R, Kiselev P, Scott G, O'Sullivan MJ, VanDyke R, Bey M, Shearer W, Jacobson RL, Jimenez E, O'Neill E, Bazin B, Delfraissy JF, Culnane M, Coombs R, Elkins M, Moye J, Stratton P, Balsley J. 1994. Reduction of maternal-infant transmission of human immunodeficiency virus type 1 with zidovudine treatment. N Engl J Med 331:1173–1180.

Darnowski JW, Goulette FA. 1994. 3'-Azido-3'-deoxythymidine cytotoxicity and metabolism in the human colon tumor cell line HCT-8. Biochem Pharmacol 48:1797–1805.

Diwan BA, Riggs CW, Logsdon D, Haines DC, Olivero OA, Rice JM, Yuspa SH, Poirier MC, Anderson LM. 1999. Multiorgan transplacental and neonatal carcinogenicity of 3'-azido-3'-deoxythymidine in mice. Toxicol Appl Pharmacol 161:82–99.

Gonzales-Cid M, Larripa I. 1994. Genotoxicity of azidothymidine (AZT) in in vitro systems. Mutat Res 321:113–118.

Helleday T. 2003. Pathways for mitotic homologous recombination in mammalian cells. Mutat Res 532:103–115.

Honma M. 2005. Generation of loss of heterozygosity and its dependency on p53 status in human lymphoblastoid cells. Environ Mol Mutagen 45:162–176.

Honma M, Zhang LS, Hayashi M, Takeshita K, Nakagawa Y, Tanaka N, Sofuni T. 1997. Illegitimate recombination leading to allelic loss and unbalanced translocation in p53-mutated human lymphoblastoid cells. Mol Cell Biol 17:4774–4781.

Honma M, Momose M, Tanabe H, Sakamoto H, Yu Y, Little JB, Sofuni T, Hayashi M. 2000. Requirement of wild-type p53 protein for maintenance of chromosomal integrity. Mol Carcinog 28:203–214.

Honma M, Momose M, Sakamoto H, Sofuni T, Hayashi M. 2001. Spindle poisons induce allelic loss in mouse lymphoma cells through mitotic non-disjunction. Mutat Res 493:101–114.

Honma M, Izumi M, Sakuraba M, Tadokoro S, Sakamoto H, Wang W, Yatagai F, Hayashi M. 2003. Deletion, rearrangement, and gene conversion; genetic consequences of chromosomal double-strand breaks in human cells. Environ Mol Mutagen 42:288–298.

Hozier J, Sawyer J, Moore M, Howard B, Clive D. 1981. Cytogenetic analysis of the L5178Y/Tk$^{+/-}$ → Tk$^{-/-}$ mouse lymphoma mutagenesis assay system. Mutat Res 84:169–181.

Jackson SP. 2002. Sensing and repairing DNA double-strand breaks. Carcinogenesis 23:687–696.

Joseph G, Grist S, Firgaira F, Turner D, Morley A. 1993. Classification of mutations at the HLA-A locus by use of the polymerase chain reaction. Environ Mol Mutagen 22:152–156.

Kennedy I, Williams S. 2000. Occupational exposure to HIV, post-exposure prophylaxis in healthcare workers. Occup Med 50:387–391.

Khanna KK, Jackson SP. 2001. DNA double-strand breaks: Signaling, repair and the cancer connection. Nat Genet 27:247–254.

Lasko D, Cavenee W. 1991. Loss of constitutional heterozygosity in human cancer. Annu Rev Genet 25:281–314.

Liber HL, Yandell DW, Little JB. 1989. A comparison of mutation induction at the Tk and Hprt loci in human lymphoblastoid cells; quantitative differences are due to an additional class of mutations at the autosomal Tk locus. Mutat Res 216:9–17.

Liechty MC, Crosby H Jr, Murthy A, Davis LM, Caspary WJ, Hozier JC. 1996. Identification of a heteromorphic microsatellite within the thymidine kinase gene in L5178Y mouse lymphoma cells. Mutat Res 371:265–271.

Meng Q, Su T, Olivero OA, Poirier MC, Shi X, Ding X, Walker VE. 2000a. Relationships between DNA incorporation, mutant frequency, and loss of heterozygosity at the TK locus in human lymphoblastoid cells exposed to 3'-Azido-3'-deoxythymidine. Toxicol Sci 54:322–329.

Meng Q, Grosovsky AJ, Shi X, Walker VE. 2000b. Mutagenicity and loss of heterozygosity at the APRT locus in human lymphoblastoid cells exposed to 3'-azido-3'-deoxythymidine. Mutagen 15:405–410.

Meng Q, Su T, O'Neill JP, Walker VE. 2002. Molecular analysis of mutations at the HPRT and TK loci of human lymphoblastoid cells after combined treatments with 3'-azido-3'-deoxythymidine and 2',3'-dideoxyinosinedagger. Environ Mol Mutagen 39:282–295.

Mittelstaedt RA, Von Tungeln LS, Shaddock JG, Dobrovolsky VN, Beland FA, Heflich RH. 2004. Analysis of mutations in the Tk gene of Tk$^{(+/-)}$ mice treated as neonates with 3'-azido-3'-deoxythymidine (AZT). Mutat Res 547:63–69.

Moore MM, Clive D, Hozier JC, Howard BE, Batson AG, Turner NT, Sawyer J. 1985. Analysis of trifluorothymidine-resistant (TFTr) mutants of L5178Y/TK$^{+/-}$ mouse lymphoma cells. Mutat Res 151:161–174.

Moore MM, Harrington-Brock K, Doerr CL, Dearfield KL. 1989. Differential mutant quantitation at the mouse lymphoma Tk and CHO Hgprt loci. Mutagen 4:394–403.

Moore MM, Honma M, Clements J, Bolcsfoldi G, Burlinson B, Cifone M, Clarke J, Delongchamp R, Durward R, Fellows M, Gollapudi B, Hou S, Jenkinson P, Lloyd M, Majeska J, Myhr B, O'Donovan M, Omori T, Riach C, San R, Stankowski LF Jr, Thakur AK, Van Goethem F, Wakuri S, Yoshimura I. 2006. Mouse lymphoma thymidine kinase gene mutation assay: Follow-up meeting of the International Workshop on Genotoxicity Testing–Aberdeen, Scotland, 2003–Assay acceptance criteria, positive controls, and data evaluation. Environ Mol Mutagen 47:1–5.

NIH. 2004. Public Health Service Task Force Recommendations for Use of Antiretroviral Drugs in Pregnant HIV-1-Infected Women for Maternal Health and Interventions to Reduce Perinatal HIV-1 Transmission in the United States. Also available at http://aidsinfo.nih.gov/guidelines/

Olivero OA, Beland F A, Poirier MC. 1994. Immunofluroscent localization and quantitiation of 3'-azido-3'-deoxythymidine (AZT) incorporated into chromosomal DNA of human, hamster, and mouse cell lines. Int J Oncol 4:449–454.

Olivero OA, Anderson LM, Diwan BA, Haines DC, Harbaugh SW, Moskal TJ, Jones AB, Rice JM, Riggs CW, Logsdon D, Yuspa SH, Poirier MC. 1997. Transplancental effects of 3'-azido-2',3'-dideoxythymidine(AZT): Tumorigenicity in mice and genotoxicity in mice and monkeys. J Natl Cancer Inst 89:1602–1608.

Olivero OA, Shearer GM, Chougnet CA, Kovacs AA, Landay AL, Baker R, Stek AM, Khoury MM, Proia LA, Kessler HA, Sha BE, Tarone RE,

Environmental and Molecular Mutagenesis. DOI 10.1002/em

AZT-Induced Deletion   257

Poirier MC. 1999. Incorporation of zidovudine into leukocyte DNA from HIV-1-positive adults and pregnant women, and cord blood from infants exposed in utero. AIDS 13:919–925.

Pastink A, Eeken JC, Lohman PH. 2001. Genomic integrity and the repair of double-strand DNA breaks. Mutat Res 481:37–50.

Poirier MC, Patterson TA, Slikker W Jr, Olivero OA. 1999. Incorporation of 3'-azido-3'-deoxythymidine (AZT) into fetal DNA, fetal tissue distribution of drug after infusion of pregnant late-term rhesus macaques with a human-equivalent AZT dose. J Acquir Immune Defic Syndr 22:477–483.

Ponomareva ON, Rose JA, Lasarev M, Rasey J, Turker MS. 2002. Tissue-specific deletion and discontinuous loss of heterozygosity are signatures for the mutagenic effects of ionizing radiation in solid tissues. Cancer Res 62:1518–1523.

Rathmell WK, Chu G. 1998. Mechanisms for DNA double-strand break repair in eukaryotes. In: Nickoloff JA, Hoekstra MF, editors. DNA Damage and Repair, Vol. 2. Totowa, NJ: Humana press. pp. 299–316.

Sargent RG, Brenneman MA, Wilson JH. 1997. Repair of site-specific double-strand breaks in a mammalian chromosome by homologous and illegitimate recombination. Mol Cell Biol 17:267–277.

Sawyer JR, Binz RL, Wang J, Moore MM. 2005. Multicolor spectral karyotyping of the L5178Y/Tk$^{-/-}$ 3.7.2C mouse lymphoma cell line. Environ Mol Mutatgen 47:127–131.

Storer RD, Kraynak AR, McKelvey TW, Elia MC, Goodrow TL, DeLuca JG. 1997. The mouse lymphoma L5178Y Tk$^{-/-}$ cell line is heterozygous for a codon 170 mutation in the p53 tumor suppressor gene. Mutat Res 373:157–165.

Sussman HE, Olivero OA, Meng Q, Pietras SM, Poirier MC, O'Neill JP, Finette BA, Bauer MJ, Walker VE. 1999. Genotoxicity of 3'-azido-3'-dideoxythymidine in the human lymphoblastoid cell line, TK6: Relationships between DNA incorpration, mutant frequency, and spectrum of deletion mutations in HPRT. Mutat Res 429:249–259.

Thiagalingam S, Foy RL, Cheng KH, Lee HJ, Thiagalingam A, Ponte JF. 2002. Loss of heterozygosity as a predictor to map tumor suppressor genes in cancer: Molecular basis of its occurrence. Curr Opin Oncol 14:65–72.

Turker MS, Gage BM, Rose JA, Elroy D, Ponomareva ON, Stambrook PJ, Tischfield JA. 1999. A novel signature mutation for oxidative damage resembles a mutational pattern found commonly in human cancers. Cancer Res 59:1837–1839.

UNAIDS. 2005. Global summary of the HIV, AIDS epidemic in 2004. Also available at http://www.unaids.org

Vazquez-Padua MA, Starnes MC, Cheng YC. 1990. Incorporation of 3'-azido-3'-deoxythymidine into cellular DNA, its removal in a human leukemic cell line. Cancer Commun 2:55–62.

Veal GJ, Back DJ. 1995. Metabolism of Zidovudine. Gen Pharmacol 26: 1469–1475.

Von Tungeln LS, Hamilton LP, Dobrovolsky VN, Bishop ME, Shaddock JG, Heflich RH, Beland FA. 2002. Frequency of TK, Hprt lymphocyte mutants and bone marrow micronuclei in B6C3F1/TK$^{-/-}$ mice treated with zidovudine and lamivudine. Carcinogenesis 23:1427–1432.

Von Tungeln LS, Williams LD, Doerge DR, Shaddock JG, McGarrity LJ, Morris SM, Mittelstaedt RA, Heflich RH, Beland FA. 2007. Transplacental drug transfer and frequency of Tk and Hprt lymphocyte mutants and peripheral blood micronuclei in mice treated transplacentally with zidovudine and lamivudine. Environ Mol Mutagen 48:258–269.

Wijnhoven SW, Van Sloun PP, Kool HJ, Weeda G, Slater R, Lohman PH, Van Zeeland AA, Vrieling H. 1998. Carcinogen-induced loss of heterozygosity at the Aprt locus in somatic cells of the mouse. Proc Natl Acad Sci USA 95:13759–13764.

Wijnhoven SW, Kool HJ, Van Teijlingen CM, Van Zeeland AA, Vrieling H. 2001. Loss of heterozygosity in somatic cells of the mouse. An important step in cancer initiation? Mutat Res 473:23–36.

Zhang LS, Honma M, Matsuoka A, Suzuki T, Sofuni T, Hayashi M. 1996. Chromosome painting analysis of spontaneous and methyl methanesulfonate-induced trifluorothymidine-resistant L5178Y cell colonies. Mutat Res 370:181–190.

Zhu C, Johansson M, Karlsson A. 2000. Incorporation of nucleoside analogs into nuclear or mitochondrial DNA is determined by the intracellular phosphorylation site. J Biol Chem 275:26727–26731.

Two-dimensional electrophoresis of protein from cultured postimplantation rat embryos for developmental toxicity studies

Makoto Usami [a,*], Katsuyoshi Mitsunaga [b], Ken Nakazawa [a]

[a] Division of Pharmacology, National Institute of Health Sciences, 1-18-1, Kamiyoga, Setagaya, Tokyo 158-8501, Japan
[b] School of Pharmaceutical Sciences, Toho University, Japan

Abstract

A simple method for two-dimensional electrophoresis (2-DE) of rat embryonic protein was described. Rat embryos cultured for 24 h from day 10.5 of gestation were used as protein samples. Protein samples were lysed in rehydration buffer and separated by isoelectric focusing with immobilized pH gradient for the first dimension and by sodium dodecyl sulfate–polyacrylamide gel electrophoresis for the second dimension. The use of the DeStreak Reagent as an antioxidant in the lysis buffer and electrode pads in the isoelectric focusing greatly improved the 2-DE pattern. When an embryo was used as a protein sample, about 800 protein spots were detected by silver staining in a 2-DE gel of the standard format. Eighty-one protein spots were identified by mass spectrometry for a primary 2-DE map. The same method could be applied to yolk sac membranes from the cultured embryos. The present method was considered to be suitable for a concomitant 2-DE analysis in in vitro developmental toxicity studies.
© 2006 Elsevier Ltd. All rights reserved.

Keywords: Two-dimensional electrophoresis; Rat; Embryo; Yolk sac; Developmental toxicity; Proteome

1. Introduction

Recent advances in two-dimensional electrophoresis (2-DE) made it possible to analyze the changes in protein expression pattern caused by exogenous stimulations in various tissues, such as the liver (Fountoulakis et al., 2000), kidney (Xu et al., 2005) and blood components (Piubelli et al., 2005). In developmental toxicity studies, the analysis of embryonic protein expression pattern by 2-DE is considered to be useful for the mechanism-based evaluation of developmental toxicants.

On the other hand, it is expected that the cultured rat embryos can be better protein samples for the analysis of

protein expression pattern in developmental toxicity studies. Postimplantation rat embryo culture is now widely used in developmental toxicity studies, by which embryos can be exposed to test chemicals under controlled conditions with a small number of animals and a small amount of test chemicals (Schmid et al., 1997).

However, there have been no suitable 2-DE methods for the analysis of embryonic protein expression pattern since most methods are for radio-labeled proteins but not for total proteins (Baumgartner et al., 1994; Praxmayer et al., 1992). The standard 2-DE methods that we tried could not be applicable because of a high salt concentration and poor solubility of embryonic samples. A method reported for the proteome analysis of mouse embryos is not considered suitable for routine analysis in developmental toxicity studies because of troublesome pretreatment of embryo samples, i.e., water-wash and dry-ice freezing (Greene et al., 2002).

In the present study, we described a simple 2-DE method for the analysis of cultured postimplantation rat embryos. By our method about 800 protein spots were detected in a

---

Abbreviations: 2-DE, two-dimensional electrophoresis; IEF, isoelectric focusing; IPG, immobilized pH gradient; SDS, sodium dodecyl sulfate; PAGE, polyacrylamide gel electrophoresis.
* Corresponding author. Tel.: +81 3 3700 1141x342; fax: +81 3 3707 6950.
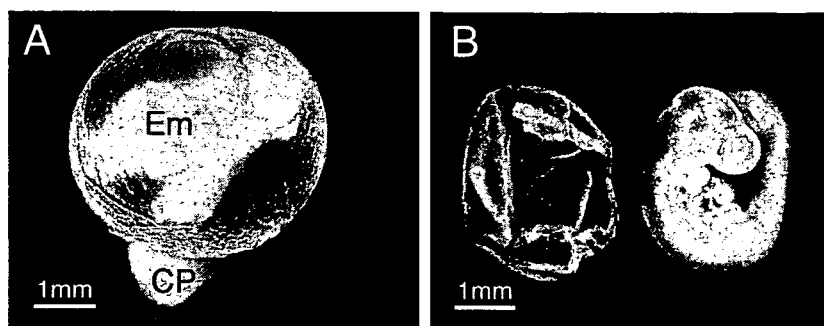E-mail address: usami@nihs.go.jp (M. Usami).

Fig. 1. Appearance of a rat embryo cultured for 24 h from day 10.5 of gestation: (A) At the end of culture. Em, embryo; YS, yolk sac; CP, chorio-allantoic placenta. (B) After the separation of embryonic membranes. Left: yolk sac membrane, Right: embryo.

single gel. The protein spots were identified by mass spectrometry for the construction of a primary 2-DE map of cultured postimplantation rat embryos. The same method could be applied to the 2-DE analysis of yolk sac membranes.

2. Materials and methods

2.1. Embryo culture

Rat embryos were cultured for 24 h by the roller bottle method as previously described (Usami and Ohno, 1996). Embryos were explanted from pregnant Wistar rats (Crlj: WI, Charles River Laboratories Japan, Inc., Kanagawa, Japan) at day 10.5 of gestation (plug day = day 0.5) under ether anesthesia. Explanted embryos were placed in a culture bottle at one embryo per 0.8–1 ml of rat serum and rotated at 35 rpm for 24 h at 37–38 °C. After the culture, the embryos and yolk sac membranes were washed three times with ice-cold buffer (0.01 M Tris–HCl, pH 7.0, 0.15 M NaCl), and placed in 1.5-ml eppendorf tubes individually with a minimum amount of the buffer for storage at −80 °C.

2.2. Preparation of embryo or yolk sac membrane samples

For 2-DE, frozen embryos or yolk sac membranes were lysed in 300 μl of rehydration buffer consisting of 7 M urea, 2 M thiourea, 2% (w/v) CHAPS, 2% (w/v) SB-10, 0.5% (v/v) IPG buffer (Amersham Biosciences, Piscataway, NJ) and 0.12% (v/v) DeStreak Reagent (Amersham Biosciences), by pulsed sonication with a 7-mm ∅ tip immediately after the addition of the buffer. Care was taken to avoid heating and forming during the sonication. Embryo or yolk sac membrane lysates were kept at 20 °C and their protein concentration was determinded with the 2D Quant Kit (Amersham Biosciences).

2.3. Isoelectric focusing (IEF) for the first dimension of 2-DE

IEF was carried out on 13-cm immobilized pH gradient (IPG) strips (Immobiline DryStrip pH 3–10 NL, Amer-

sham Biosciences) with the IPGphor system (Amersham Biosciences). IPG strips were rehydrated with the rehydration buffer containing 50 μg protein of embryo or yolk sac membrane lysate for at least 12 h at 20 °C under a cover with silicon oil. Before the start of IEF, 3-mm-wide IEF electrode strips (Amersham Biosciences) damped were inserted between the IPG strip and both electrodes as electrode pads. Electrophoresis conditions were – Step 1: Step-n-hold at 500 V for 1 h, Step 2: Gradient at 1000 V for 1 h, Step 3: Gradient 8000 V for 2.5 h with the current limit of 50 μA per IPG strip. When electrophoresis for the second dimension was not carried out immediately after IEF, the IPG strips were stored at −80 °C.

2.4. Sodium dodecyl sulfate–polyacrylamide gel electrophoresis (SDS–PAGE) for the second dimension of 2-DE

SDS–PAGE was performed according to the method of Laemmli (Laemmli, 1970) except that no stacking gel was used. After IEF, IPG strips were equilibrated with 5 ml of SDS equilibration buffer consisting of 0.05 M Tris–HCl, pH 8.8, 6 M urea, 30% (v/v) glycerol, 2% (w/v) SDS, 0.025% (w/v) bromophenol blue. For the first equilibration, IPG strips were placed in a tube containing equilibration buffer with dithiothreitol (50 mg/5 ml) and rocked for 20 min. For the second equilibration, IPG strips were placed in a tube containing equilibration buffer with iodoacetamide (125 mg/5 ml) and rocked for 20 min. Equilibrated IPG strips were applied onto polyacrylamide gels (12.5% T, 2.6% C, 14 × 6 cm) and sealed with 0.5% agarose in electrode buffer. Electrophoresis was carried at a constant current of

Table 1
Size and protein content of cultured rat embryos

Item	Mean	Standard deviation
Yolk sac diameter (mm)	4.37	0.10
Crown-rump length (mm)	3.99	0.16
Number of somite pairs	26.0	0.67
Embryo protein (μg)	298.2	31.0
Yolk sac protein (μg)	153.0	20.2

Values for 10 embryos are shown.

10 mA per gel for 15 min and thereafter 20 mA per gel until the dye front reached the edge of the gel.

2.5. Stain of 2-DE gel and protein identification

After SDS–PAGE, 2-DE gels were stained with the Plus One Silver Staining Kit Protein (Amersham Biosciences) using the Multi Processor (Amersham Biosciences) according to the manufacturer's instruction. Stained 2-DE gels were scanned and analyzed with the PD Quest 2D analysis software (Bio-Rad, Hercules, CA).

For the identification of protein spots by mass spectrometry, 2-DE gels were stained with the mass-analysis compatible Proteo Silver staining kit (Sigma, St. Louis, MO) and protein spots were excised and cut into 1-mm cubes with a scalpel. Proteins in the gel cubes were digested with trypsin (Shevchenko et al., 1996), cleaned-up with Zip-Tip C18μ (Millipore, Bedford, MA) and analyzed by mass spectrometry using the 4700 Proteomics Analyzer (Applied Biosystems, Foster City, CA). The proteins were identified by the use of mass spectrometry data for the search of primary

sequence databases with the MS/MS ion search mode of the Mascot search engine (Matrix Science, Boston, MA).

3. Results

3.1. Embryo culture

Fig. 1A shows a cultured rat embryo at the end of the 24-h culture period. Embryos and yolk sac membranes were separated as samples for 2-DE analysis (Fig. 1B). The amnion and chorio-allantoic placenta were removed and discarded. The size and protein content of the embryos and yolk sac membranes of the cultured rat embryos are shown in Table 1. Protein content in the individual embryo or yolk sac membrane was sufficient for 2-DE anaylsis.

3.2. 2-DE of embryo protein

Proteins of cultured embryos were well separated by 2-DE with the present method (Fig. 2). About 800 protein spots were consistently detected in replicate gels each
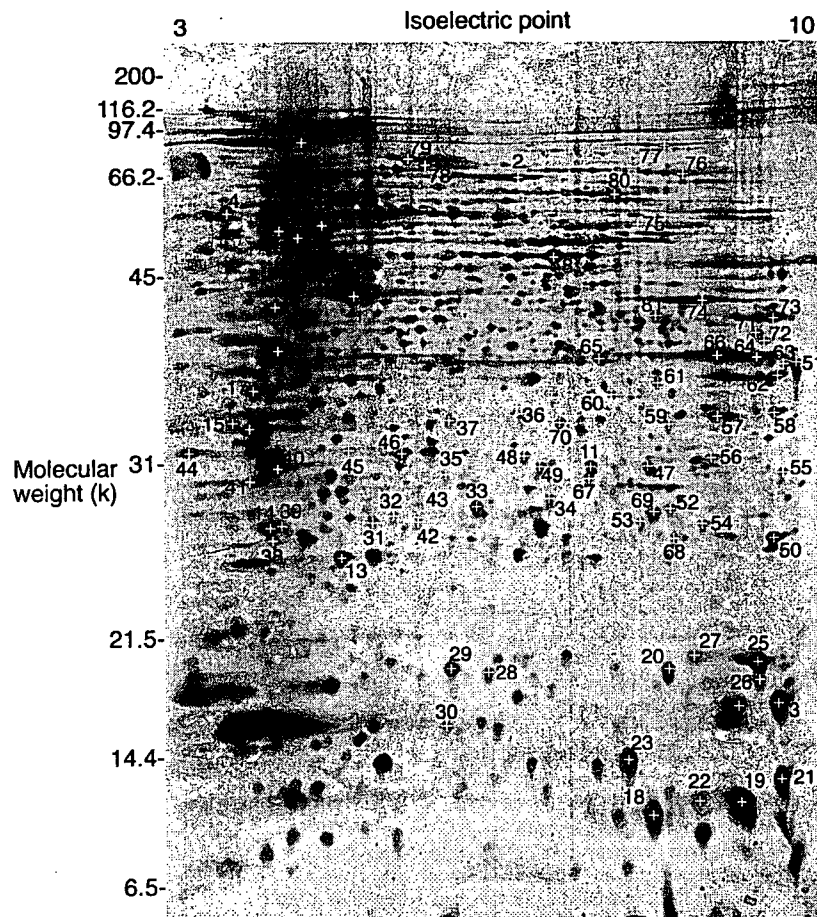

Fig. 2. 2-DE pattern of embryo proteins from a cultured rat embryo equivalent to day 11.5 of gestation. Proteins (50 μg) were separated by IEF with 3–10NL IPG strip (13 cm) and by SDS–PAGE with 12.5% gel (14 × 6 cm), and were stained with silver. Identified protein spots were numbered and listed in Table 2.

Table 2
Protein spots identified in the 2-DE of embryo protein

Spot no.	Accession no.	Protein name	Nominal mass	Calculated pI
1	gi|71620	Actin beta	42,066	5.29
2	gi|19705431	Albumin	70,670	6.09
3	gi|37748460	Peptidylprolyl isomerase A	18,091	8.34
4	gi|11693172	Calreticulin	48,137	4.33
5	gi|202549	Iodothyronine 5′ monodeiodinase	54,375	4.87
6	gi|38014578	Tubulin, beta, 2	50,225	4.79
7	gi|54792127	ATP synthase, H$^+$ transporting, mitochondrial F1 complex, beta subunit	56,318	5.19
8	gi|38649320	Enol protein	51,736	6.70
9	gi|38014840	Laminin receptor 1	32,917	4.80
10	gi|112077	Nucleolar phosphoprotein B23.1	32,711	4.62
11	gi|12844989	Unnamed protein product	28,799	6.67
12	gi|51859516	Heat shock 90 kDa protein 1, beta	83,631	4.97
13	gi|8394432	Peroxiredoxin 2	21,941	5.34
14	gi|6678437	Tumor protein, translationally-controlled 1	19,564	4.76
15	gi|48675371	Complement component 1, q subcomponent binding protein	31,320	4.77
16	gi|34876714	Predicted: similar to Eukaryotic translation elongation factor 1 beta 2	24,831	4.55
17	gi|7242171	Proliferating cell nuclear antigen	29,108	4.66
18	gi|27668426	Predicted: similar to hemoglobin: Subunit = zeta	16,124	6.75
19	gi|3367724	Epsilon 1 globin	16,151	7.90
20	gi|55926145	Expressed in non-metastatic cells 2	17,386	6.92
21	gi|1628436	Profilin	15,149	8.46
22	gi|3367724	Epsilon 1 globin	16,151	7.90
23	gi|40254577	Ribosomal protein S12	14,905	6.81
24	gi|37748460	Peptidylprolyl isomerase A	18,091	8.34
25	gi|509201	Cofilin	18,749	8.22
26	gi|7441446	Destrin	18,661	7.78
27	gi|6671746	Cofilin 2, muscle	18,812	7.66
28	gi|19924089	Expressed in non-metastatic cells 1, protein (NM23A) (nucleoside diphosphate kinase)	17,296	5.96
29	gi|38328242	Stmn1 protein	17,278	5.76
30	gi|12850597	Unnamed protein product	17,138	5.95
31	gi|57006	Unnamed protein product	22,320	5.55
32	gi|202945	Apolipoprotein A-I precursor	30,100	5.52
33	gi|3688521	Thiol-specific antioxidant protein	24,860	5.64
34	gi|8394082	Proteasome (prosome, macropain) subunit, beta type 3	23,235	6.15
35	gi|20071222	NADH dehydrogenase (ubiquinone) Fe-S protein 3	30,358	6.40
36	gi|1381643	Cysteine protease p32-beta	30,097	5.68
37	gi|30410794	Proteasome activator subunit 3 isoform 1	29,602	5.69
38	gi|21312044	Eukaryotic translation initiation factor 3, subunit 12	25,356	4.81
39	gi|6671696	Chromobox homolog 1 (Drosophila HP1 beta)	21,519	4.85
40	gi|27664664	Predicted: similar to 25 kda FK506-binding protein	25,220	9.29
41	gi|6381991	Integrin beta 4 binding protein	27,007	4.63
42	gi|202945	Apolipoprotein A-I precursor	30,100	5.52
43	gi|2897818	Huntingtin interacting protein-2	22,503	5.33
44	gi|6978499	Acidic (leucine-rich) nuclear phosphoprotein 32 family, member A	28,718	3.99
45	gi|47169488	TPA: proteasome subunit alpha type 3-like	28,621	5.19
46	gi|62664759	Predicted: prohibitin	27,757	5.44
47	gi|297111	Phosphoglyceromutase	28,908	8.85
48	gi|16758298	Proteasome (prosome, macropain) subunit, beta type 7	30,250	8.13
49	gi|16758848	Endoplasmic retuclum protein 29	28,614	6.23
50	gi|56789700	Peroxiredoxin 1	22,323	8.27
51	gi|38648863	Malate dehydrogenase, mitochondrial	36,117	8.93
52	gi|16758182	RAN, member RAS oncogene family	24,579	7.01
53	gi|5420030	Glutathione transferase	25,550	6.77
54	gi|25453420	Glutathione S-transferase, pi	23,652	6.89
55	gi|56550075	Proteasome (prosome, macropain) subunit, alpha type 7	28,010	8.60
56	gi|8394069	Proteasome (prosome, macropain) subunit, alpha type 4	29,764	7.59
57	gi|18543331	Guanine nucleotide binding protein, beta polypeptide 2-like 1	35,529	7.60
58	gi|38051979	Vdac1 protein	32,060	8.35
59	gi|1906812	Inducible carbonyl reductase	30,920	7.64
60	gi|62661724	Predicted: similar to esterase D/formylglutathione hydrolase	37,322	6.45

Table 2 (continued)

Spot no.	Accession no.	Protein name	Nominal mass	Calculated pI
61	gi|57527447	Ribose-phosphate pyrophosphokinase I -like	35,297	6.51
62	gi|54261548	Lactate dehydrogenase A	36,712	8.45
63	gi|7949053	Heterogeneous nuclear ribonucleoprotein A2/B1 isoform 1	36,028	8.67
64	gi|62653546	Predicted: similar to glyceraldehyde-3-phosphate dehydrogenase	36,045	8.44
65	gi|6978491	Aldehyde reductase 1	36,230	6.26
66	gi|62653546	Predicted: similar to glyceraldehyde-3-phosphate dehydrogenase	36,045	8.44
67	gi|76647405	Predicted: similar to proteasome subunit alpha type 6 (proteasome iota chain) (macropain iota chain)	27,838	6.34
68	gi|8394079	Proteasome (prosome, macropain) subunit, beta type 2	23,069	6.96
69	gi|8394063	Proteasome (prosome, macropain) subunit, alpha type 2	26,024	6.92
70	gi|62655706	Predicted: similar to RIKEN cdna 1110025F24	26,482	5.90
71	gi|61889115	Phosphoserine aminotransferase 1	40,943	7.57
72	gi|66911068	Pcbp2_predicted protein	35,666	8.17
73	gi|202837	Aldolase A	39,691	8.31
74	gi|38649310	Phosphoglycerate kinase 1	44,909	8.02
75	gi|584875	Adenylyl cyclase-associated protein 1 (CAP 1)	51,857	7.16
76	gi|74144333	Unnamed protein product	67,573	7.18
77	gi|19424312	KH-type splicing regulatory protein	74,466	6.38
78	gi|228784	Alpha fetoprotein	70,167	5.71
79	gi|228784	Alpha fetoprotein	70,167	5.71
80	gi|2511703	p60 protein	63,158	6.40
81	gi|2644966	hnRNP-E1 protein	37,987	6.66

Proteins names with their NCBI accession numbers were shown for the protein spots in Fig. 1.

from one embryo. Selected protein spots were analyzed by mass spectrometry and 81 protein spots were identified as shown in Table 2. These protein spots also served as landmarks for the matching of protein spots among the gels.

3.3. 2-DE of yolk sac membrane protein

Proteins of yolk sac membranes were separated as well as those of embryos by 2-DE with the present method (Fig. 3). The 2-DE pattern of yolk sac membranes was fairly different from that of embryos. Most protein spots were common but were quantitatively different between the yolk sac membranes and the embryos. In addition, there were embryo specific and yolk sac membrane specific protein spots.

4. Discussion

The present method is simple and can be carried out concomitantly with in vitro developmental toxicity studies using rat embryo culture. The whole 2-DE procedures are completed within four days. IPG strips with narrower pH ranges would be useful for precise and convenient analysis of specific protein spots. For screening purposes or focused proteomics, the same procedures could be applied to the mini-gel format with shorter IPG strip and mini SDS–PAGE gel.

The primary 2-DE map constructed in the present study is useful for interlaboratory comparison of 2-DE patterns. Abundant and characteristic protein spots can be used as landmarks for matching of the 2-DE pattern. We are planning to identify more protein spots for a more precise and

accurate 2-DE map of cultured rat embryos in future, giving priority to protein spots of interest that are differentially expressed due to the effects of developmental toxicants. Identification of very faint protein spots may require a separate 2-DE experiment with an increased amount of applied protein samples.

It is expected that 2-DE analysis by the present method enables informative experiments for developmental toxicity studies. Because protein from less than one embryo is sufficient for 2-DE analysis in the present method, toxic effects observed in individual embryos may be related to the changes in protein expression pattern. Alternatively, analysis of specific parts isolated from single embryos may improve the efficiency of differential analysis. It is also noted that the present method is valid for 2-DE analysis of yolk sac membranes as well as embryos. Simultaneous analysis of yolk sac membranes with embryos would be useful to investigate the action sites of developmental toxicants.

The critical point of the present method is the use of the DeStreak Reagent as an antioxidant and the electrode pads. Both of which greatly improved the 2-DE pattern by decreasing horizontal streaks in the present method. We initially used dithiothreitol or tributylphosphine as a reducing agent to avoid the oxidation of proteins but could not decrease the streaks sufficiently. High concentration of redox agents such as glutathione in the embryo or yolk sac membrane samples (Harris et al., 1995) might affect redox status of proteins when dithiothreitol or tributylphosphine was used.

As far as we tested, addition of protease inhibitors to the lysis/rehydration buffer had no effects on the 2-DE pattern. It is considered that the constituents of the lysis/rehydration buffer were effective for inactivation of proteases in the
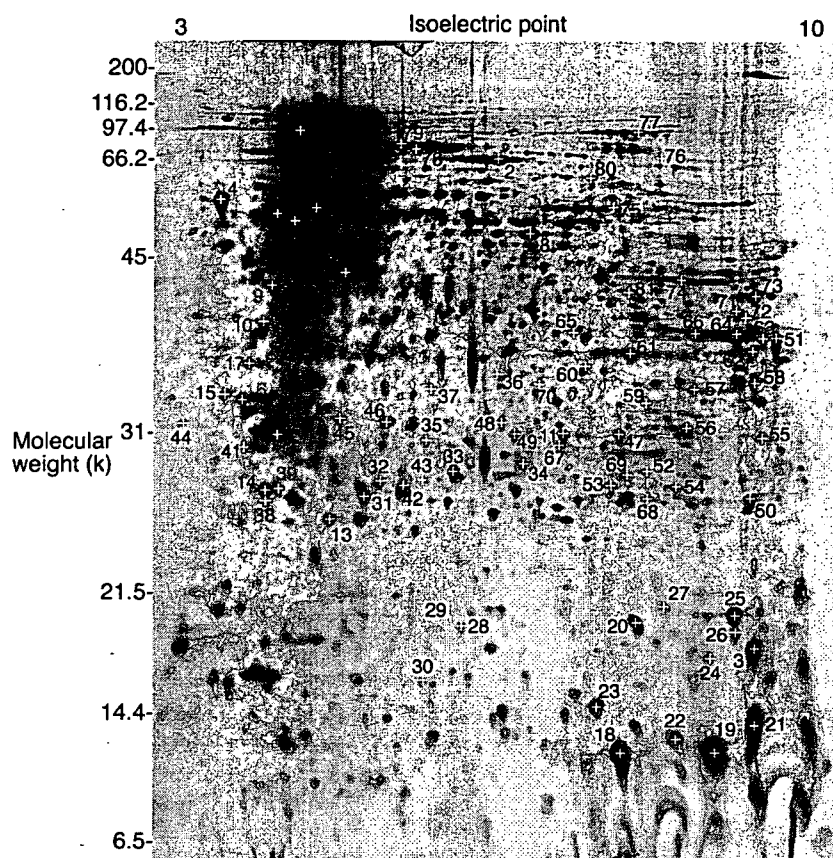
Fig. 3. 2-DE pattern of yolk sac membrane proteins from a cultured rat embryo equivalent to day 11.5 of gestation. Proteins (50 μg) were separated by IEF with 3–10NL IPG strip (13 cm) and by SDS–PAGE with 12.5% gel (14 × 6 cm), and were stained with silver. Proteins identified for the embryo are indicated by the same number as in Fig. 2.

embryo or yolk sac membrane samples. No requirement for protease inhibitors in the present method saves the const and labor in the 2-DE analysis.

In conclusion, it is considered that the present method is suitable for 2-DE analysis of embryos and yolk sac membranes in developmental toxicity studies using postimlantation rat embryo culture.

Acknowledgements

References

Baumgartner, B.G., Murach, K.-F., Schlegel, E., Praxmayer, C., Illmensee, K., 1994. Comparison of protein analysis between embryonic and extraembryonic tissues during the 11th day of gestation of the mouse. Electrophoresis 15, 992–1000.

Fountoulakis, M., Berndt, P., Boelsterli, U.A., Crameri, F., Winter, M., Albertini, S., Suter, L., 2000. Two-dimensional database of mouse liver proteins: Changes in hepatic protein levels following treatment with acetaminophen or its nontoxic regioisomer 3-acetamidophenol. Electrophoresis 21, 2148–2161.

Greene, N.D.E., Leung, K.-Y., Wait, R., Begum, S., Dunn, M.J., Copp, A.J., 2002. Differential protein expression at the stage of neural tube closure in the mouse embryo. J. Biol. Chem. 277, 41645–41651.

Harris, C., Hiranruengchok, R., Lee, E., Berberian, R.M., Eurich, G.E., 1995. Glutathione status in chemical embryotoxicity: Synthesis, turnover and adduct formation. Toxicol. in Vitro 9, 623–631.

Laemmli, U.K., 1970. Cleavage of structural proteins during the assembly of the head of bacteriophage T4. Nature 227, 680–685.

Piubelli, C., Cecconi, D., Astner, H., Caldara, F., Tessari, M., Carboni, L., Hamdan, M., Righetti, P.G., Domenici, E., 2005. Proteomic changes in rat serum, polymorphonuclear and mononuclear leukocytes after chronic nicotine administration. Proteomics 5, 1382–1394.

Praxmayer, C., Murach, K.-F., Baumgartner, B., Aberger, F., Schlegel, E., Illmensee, K., 1992. Protein synthesis in murine organs during postimplantation development detected by two-dimensional gel electrophoresis. Electrophoresis 13, 720–722.

Schmid, B., Bechter, R., Kucera, P., 1997. Use of whole emryo cultures in in vitro teratogenicity testing. In: Castell, J.V., Gómez-Lechón, M.J. (Eds.), In Vitro Methods in Pharmacetical Research. Academic Press, San Diego, pp. 353–373.

Shevchenko, A., Wilm, M., Vorm, O., Mann, M., 1996. Mass spectrometric sequencing of proteins from silver-stained polyacrylamide gels. Anal. Chem. 68, 850–858.

Usami, M., Ohno, Y., 1996. Teratogenic effects of selenium compounds on cultured postimplantation rat embryos. Teratog. Carcinog. Mutagen. 16, 27–36.

Xu, H., Hu, L.S., Chang, M., Jing, L., Zhang, X.Y., Li, G.S., 2005. Proteomic analysis of kidney in fluoride-treated rat. Toxicol. Lett. 160, 69–75.

Research Report

β-Estradiol induces synaptogenesis in the hippocampus by enhancing brain-derived neurotrophic factor release from dentate gyrus granule cells

Kaoru Sato[a,*], Tatsuhiro Akaishi[b], Norio Matsuki[c], Yasuo Ohno[a], Ken Nakazawa[a]

[a]Division of Pharmacology, National Institute of Health Sciences, 1-18-1 Kamiyoga, Setagaya-ku, Tokyo 158-8501, Japan
[b]Laboratory of Pharmacology, Faculty of Pharmacy and Research Institute of Pharmaceutical Sciences, Musashino University, 1-1-20 Shinmachi, Nishitokyo-shi, Tokyo 202-8585, Japan
[c]Laboratory of Chemical Pharmacology, Graduate School of Pharmaceutical Sciences, University of Tokyo, 7-3-1 Hongo, Bunkyo-ku, Tokyo 113-0033, Japan

ARTICLE INFO

ABSTRACT

We investigated the effect of β-estradiol (E2) on synaptogenesis in the hippocampus using organotypic hippocampal slice cultures and subregional hippocampal neuron cultures. E2 increased the expression of PSD95, a postsynaptic marker, specifically in stratum lucidum of Cornu Ammonis 3 (CA3SL) in cultured hippocampal slices. E2 also increased the spine density at the proximal site of CA3 apical dendrites in CA3SL and PSD95 was clustered on these spine heads. The effects of E2 on the expression of PSD95 and the spine density disappeared when the dentate gyrus (DG) had been excised at 1 day in vitro (DIV). FM1-43 analysis of subregional hippocampal neuron cultures which were comprised of Ammon's horn neurons, DG neurons, or a mixture of these neurons, revealed that E2 increased the number of presynaptic sites in the cultures that contained DG neurons. K252a, a potent inhibitor of the high affinity receptor of brain-derived neurotrophic factor (BDNF), and function-blocking antibody to BDNF (BDNFAB) completely inhibited the effects of E2 in hippocampal slice cultures and subregional neuron cultures, whereas ICI182,780 (ICI), a strong antagonist of nuclear estrogen receptors (nERs), did not. Expression of BDNF in DG neurons was markedly higher than that in Ammon's horn

* Corresponding author. Fax: +81 3 3707 6950.
  E-mail address: kasato@nihs.go.jp (K. Sato).

neurons and E2 did not affect these expression levels. E2 significantly increased the BDNF release from DG neurons. KT5720, a specific inhibitor of 3'-5'-cyclic adenosine monophosphate (cAMP)-dependent protein kinase A (PKA), and Rp-adenosine 3', 5'-cyclic monophosphorothioate triethylammonium salt (Rp-cAMP), a non-hydrolyzable diastereoisomer and a potent inhibitor of PKA, completely suppressed the E2-induced increase in BDNF release, whereas ICI and U0126, a potent inhibitor of MAP kinase kinase (MEK), did not. These results suggest that E2 induces synaptogenesis between mossy fibers and CA3 neurons by enhancing BDNF release from DG granule cells in a nER-independent and PKA-dependent manner.

1. Introduction

Estrogens have diverse effects on structure and function of the central nervous system (CNS) (for review, McEwen et al., 2001; Scharfman and MacLusky, 2005; Segal and Murphy, 2001). These effects include enhancement of glutamate-mediated transmission (Woolley, 1998), decreased afterhyperpolarization (Kramar et al., 2004), facilitation of memory (Tyler et al.,

2002), increased dendritic spine and spine synapse numbers (Segal and Murphy, 2001), promotion of DG neurogenesis (Tanapat et al., 1999), and increased seizure susceptibility (Woolley and Schwartzkroin, 1998). Such diversity arises because estrogens have multiple mechanisms of action. They modulate gene transcription by interacting with 2 types of nERs, ERα and ERβ. In addition, recent reports clarified nongenomic mechanisms that act via receptors associated
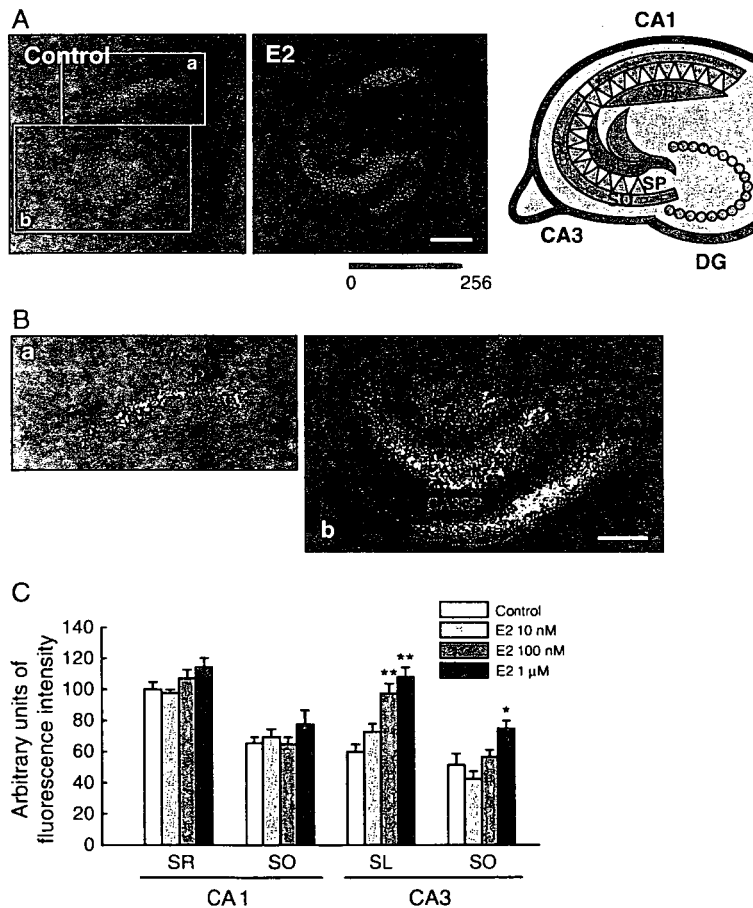

Fig. 1 – Effects of E2 on the expression of PSD95 in cultured hippocampal slices. (A) PSD95 immunoreactive signals in the control slice (left) and the slice treated with E2 (1 μM, 24 h) (middle). Bar=500 μm. (B) Magnified gray-scale images of a and b in A. CA1SR, CA1SO, CA3SL, and CA3SO appeared as fluorescent compartments. Bar=250 μm. (C) Effects of E2 (10 nM-1 μM, 24 h) on the expression of PSD95. E2 increased the expression level of PSD95 dose-dependently in CA3SL. *: $p<0.05$, **: $p<0.01$ vs. the control group in each region. $N=8$, Tukey's test following ANOVA.

with or integral to plasma membrane (mERs), thereby activating signaling cascades distinct from those of nERs (Beyer et al., 2003; Kelly and Levin, 2001; Segars and Driggers, 2002). We previously reported that pretreatment with estrogens increased neuronal sensitivity to L-glutamate (L-glu) specifically in CA3 in organotypic hippocampal slice cultures. In the same study we found that these effects were mediated by the mechanisms that did not involve nERs (Sato et al., 2002). These results raised the possibility that estrogens affect synaptic contacts in CA3. In the present study, we therefore investigated the effects of E2 on synaptogenesis in the hippocampus and explored the underlying mechanisms using 2 experimental systems. Firstly, we investigated the effects of E2 on the expression of PSD95, a postsynaptic marker, and the spine density in cultured hippocampal slices. Secondly, we investigated the effects of E2 on the number of presynaptic release sites in subregional hippocampal neuron cultures, which were comprised of Ammon's horn neurons, DG neurons, or a mixture of these neurons. It has been reported that in the hippocampus the highest concentration of BDNF occurs in DG granule cells, especially in their axons, mossy fibers (Dieni and Rees, 2002; Scharfman et al., 2003), from the prenatal period through to adulthood (Dieni and Rees, 2002). Although BDNF is known to promote synaptogenesis (Aguado et al., 2003; Alsina et al., 2001; Seil and Drake-Baumann, 2000), it has not been elucidated whether the BDNF in DG granule cells has a role in hippocampal synapse formation. For this reason, we also investigated the relationship between endogenous BDNF in DG granule cells and the effects of E2 in CA3. We here provide evidence showing that E2 induces synaptogenesis between mossy fibers and CA3 neurons by enhancing BDNF release from DG granule cells in a nER-independent and PKA-dependent manner.

2. Results

2.1. Effects of E2 on postsynaptic sites in cultured hippocampal slices

We first examined the effect of E2 on the expression of PSD95 in cultured hippocampal slices immunohistochemically. PSD95 is one of the PDZ (PSD-95-Disks large-zona occludens 1/2) domain-containing proteins (Craven and Bredt, 1998; Garner et al., 2000) and is an integral protein of the postsynaptic density. In the control group, the fluorescent signals for PSD95 were apparent in the major hippocampal synaptic sites, i.e., stratum radiatum (SR), stratum oriens (SO), SL and the dentate hilar region (Fig. 1A, left). Because in this study slices were cultured after removing entorhinal cortex, we quantified the expression of PSD95 in CA1SR, CA1SO, CA3SL, and CA3SO, the synaptic sites which maintain the intact presynaptic and postsynaptic cells. Because CA1SR, CA1SO, CA3SL, and CA3SO appeared as fluorescent compartments (Figs. 1B, a and b) in magnified gray-scale mode images, we regarded the averaged fluorescence intensity of each compartment (an outlined area) as the expression level of PSD95 of each synaptic site (see Experimental procedures). When we compared the effects of E2 on the PSD95 expression in CA1 and CA3, E2 (24 h) increased the expression of PSD95 dose-

dependently in CA3SL and the effects were significant at 100 nM and the higher concentration (Figs. 1A middle and B). Although E2 also increased the PSD 95 expression in CA3SO at 1 μM (145±9.75% of control), the effect was weaker than that in CA3SL (180±10.2% of control at 1 μM). The distribution pattern of PSD95 signals (including area) in each region was not affected by E2. We then investigated the effect of E2 on the spine density in CA3SL using 1,1'-dioctadecyl-3,3,3',3'-tetramethylindocarbocyanine perchlorate (DiI) staining. E2 (1 μM, 24 h) markedly increased the spine density at the proximal site of CA3 apical dendrites in CA3SL (296±24.3% of control; Figs. 2A and B). E2 also increased the spine density at the proximal site of CA1 apical dendrites in CA1SR (132±4.49% of control), although to a much lesser extent than that in CA3SL (Fig. 2A). Fig. 2B shows typical images of the proximal sites of CA3 apical dendrites in the control slice (left) and in the E2-treated slice (right). When we immunostained the E2-treated slices with anti-PSD95 antibody after DiI staining, most PSD95 signals in CA3SL clustered on the spine heads (Fig. 2B, right). These results indicate that E2 increased the number of postsynaptic sites in CA3SL. CA3SL is the region in which mossy fibers (DG granule cell axons) make synapses with CA3 pyramidal neurons. We then investigated the effect of E2 on the expression of PSD95 and the spine density in CA3 in DG (−) slices, i.e., the slices of which DG had been excised at 1 DIV. As shown by
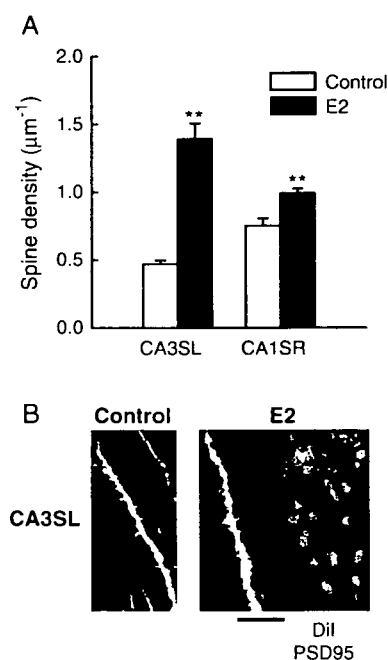

Fig. 2 – Effects of E2 on the spine density in cultured hippocampal slices. (A) E2 (1 μM, 24 h) markedly increased the spine density in CA3SL. **: p<0.01 vs. the vehicle control group in each region. N=8, Student's t test. (B) Typical images of the DiI-labeled CA3 apical dendrites in the control slice (left) and the E2-treated slice (right). Double staining with DiI and anti-PSD95 antibody revealed that in the E2-treated slice most PSD95 signals (green) were clustered on the spine-heads of the CA3 apical dendrites (red). Bar=5 μm.

Nissl staining, the viability of CA3 pyramidal neurons was not altered by the dissection of the DG (Fig. 3A). The distribution pattern of the PSD95 signals was not affected, either (Fig. 3B). E2 (1 μM, 24 h) affected neither the expression level (Fig. 3C) nor the distribution pattern of PSD95 in DG (–) slices (data not shown). The effect of E2 (1 μM, 24 h) on the spine density in CA3SL was also abolished in DG (–) slices (Fig. 3D). Taken together, these results suggest that E2 induces synaptogenesis between mossy fibers and CA3 pyramidal neurons.

2.2. Effects of E2 on presynaptic sites in subregional hippocampal neuron cultures

We next investigated the effect of E2 on the number of presynaptic sites using subregional hippocampal neuron cultures, which were comprised of Ammon's horn neurons, DG neurons, or a mixture of these neurons, respectively. We quantified the number of presynaptic sites by counting the number of sites in which depolarization-induced uptake and release of (N-(3-triethylammoniumpropyl)-4-(4-(dibutyla-mino)styryl)pyridinium dibromide (FM1-43) (Cochilla et al., 1999) had occurred (see Experimental procedures). Fig. 4A shows the typical morphologies of neurons in the Ammon's horn neuron culture (left) and in the DG neuron culture (middle). Most cells in the Ammon's horn neuron culture were large and spindle-shaped, whereas most cells in the DG neuron culture were small and granular. As shown in Fig. 4B, E2 (1 μM, 24 h) significantly increased the number of presynaptic sites in the mixed neuron culture (199±9.18% of control). E2 also increased the number of presynaptic sites in the DG neuron culture (170±12.1% of control), but not in the Ammon's horn neuron culture. Fig. 4C shows the typical fluorescent images of presynaptic sites (red puncta) in the control group (top left) and in the E2-treated group (top right) in the mixed neuron culture. We confirmed that E2 had no effect on the number of surviving neurons in each culture by immunostaining with anti-NeuN antibody (data not shown). These results indicate that E2 increased the number of presynaptic sites in the hippocampal neuron cultures and that DG neurons are indispensable for this effect.

2.3. The effects of E2 in hippocampal slice cultures and subregional hippocampal neuron cultures were mediated by the mechanism which is independent of nERs and dependent on endogenous BDNF

Pharmacological experiments were performed to investigate and compare the mechanisms underlying the effects of E2 in hippocampal slice cultures and subregional hippocampal neuron cultures (the mixed neuron culture) (Fig. 5). First, we examined the contribution of nERs using ICI, a strong antagonist to both of ERα (Ki: 1.5 nM) and ERβ (Ki: 6.4 nM) (Kuiper et al., 1997). ICI at a concentration of 1 μM did not alter the effect of E2 on the expression of PSD95 expression, the spine density, and the number of presynaptic sites (Figs. 5A–C). It has been reported that DG granule cells have the highest concentration of BDNF in the hippocampus, especially in the mossy fibers (Dieni and Rees, 2002; Scharfman et al., 2003). Because BDNF is known to enhance synapse formation (Aguado et al., 2003; Alsina et al., 2001; Seil and Drake-
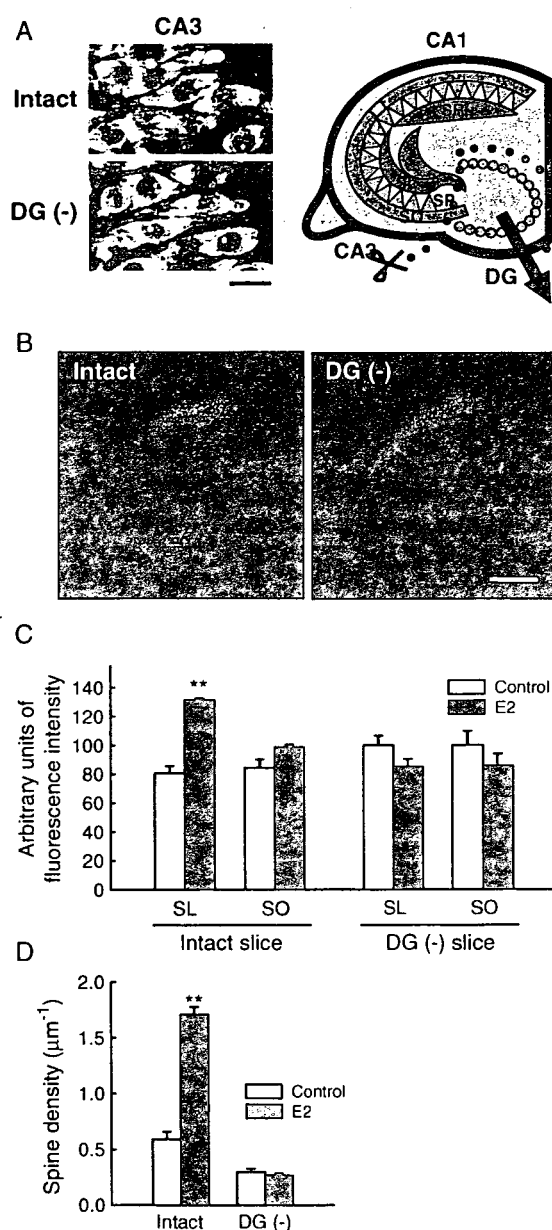

Fig. 3 – Effects of E2 on the expression of PSD95 and the spine density in cultured hippocampal slices of which DG had been excised at 1 DIV. (A) The viability of CA3 pyramidal neurons in DG (–) slices. Nissl staining revealed that their viability was not affected by the dissection of DG. Bar=20 μm. (B) Immunoreactive signals of PSD95 in a DG (–) slice. The distribution pattern of the PSD95 signals was not affected by the dissection of DG. Bar=500 μm. (C) The effect of E2 on the expression of PSD95 in DG (–) slices. E2 (1 μM, 24 h) did not affect the expression of PSD95 in CA3 in DG (–) slices. (D) The effect of E2 on the spine density in CA3SL in DG (–) slices. E2 (1 μM, 24 h) did not affect the spine density in CA3SL in DG (–) slices.

A

Ammon's horn   DG   Hippocampus

B

C

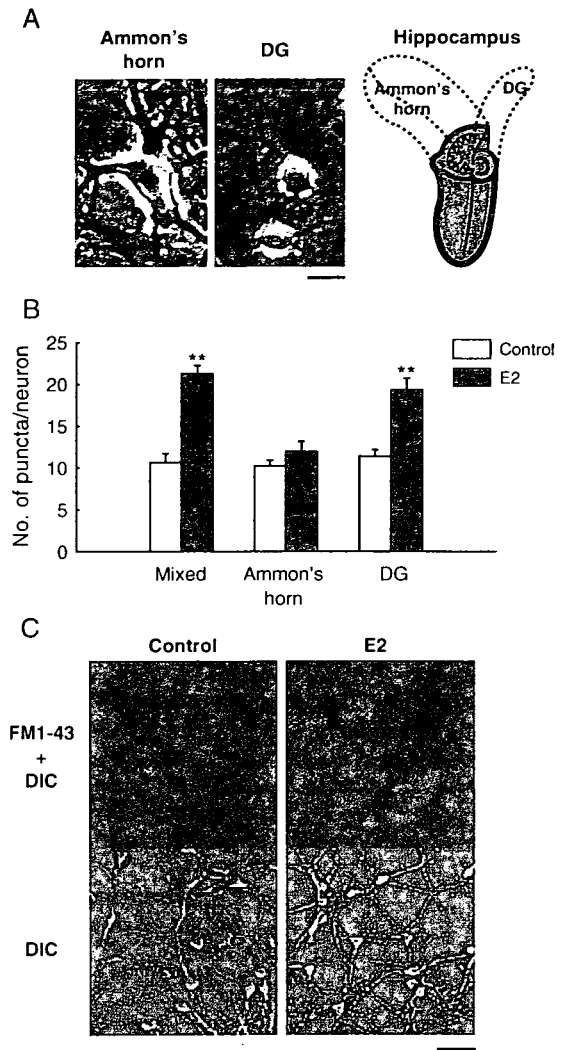Control   E2

FM1-43
+
DIC

DIC

Fig. 4 – Effects of E2 on the number of presynaptic sites in subregional hippocampal neuron cultures. (A) Typical cell morphologies in the Ammon's horn neuron culture (left) and in the DG neuron culture (middle). Bar=20 μm. (B) E2 (1 μM, 24 h) significantly increased the number of presynaptic sites in the mixed neuron culture and in the DG neuron culture. **: $p < 0.01$ vs. the control group in each culture. $N=8$, Student's t test. (C) Typical images of presynaptic sites visualized by FM1-43 (red puncta) in the control group (top left) and in the E2-treated group (top right) in the mixed neuron culture. DIC images of the same microscopic views were also shown (bottom left and bottom right). Bar=50 μm.

Baumann, 2000), we examined the involvement of BDNF in the effects of E2. K252a (200 nM), a potent inhibitor of the high affinity receptor of BDNF (TrkB) (Squinto et al., 1991; Bothwell, 1995), significantly inhibited the effects of E2 on the expression of PSD95 expression, the spine density, and the number of presynaptic sites (Figs. 5A–C). Furthermore BDNFAB (10 μg/ml)

significantly inhibited the effects of E2 in these experiments (Figs. 5A–C). These inhibitors alone had no effects in each case. These results indicate that the effects of E2 in hippocampal
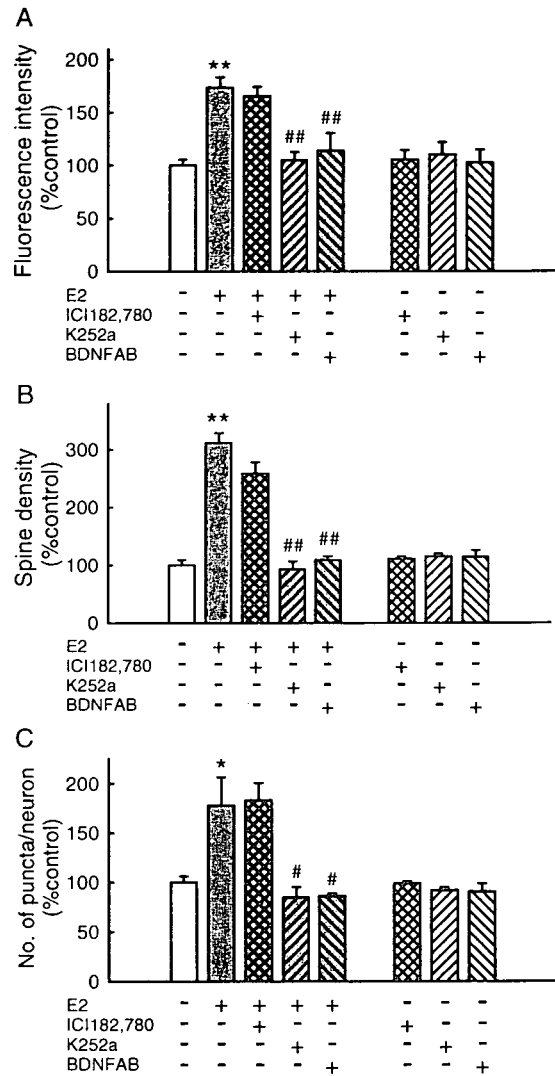
A

B

C

Fig. 5 – Effects of ICI, K252a, and BDNFAB on the effects of E2 in hippocampal slice cultures and subregional hippocampal neuron cultures. (A) K252a (200 nM) and BDNFAB (10 μg/ml) significantly inhibited the effect of E2 on the expression of PSD95 in cultured hippocampal slices, whereas ICI (1 μM) did not. **: $p < 0.01$ vs. the control group, ##: $p < 0.01$ vs. the E2-treated group. $N=8$, Tukey's test following ANOVA. (B) K252a (200 nM) and BDNFAB (10 μg/ml) significantly inhibited the effect of E2 on the spine density in cultured hippocampal slices, whereas ICI (1 μM) did not. **: $p < 0.01$ vs. the control group, ##: $p < 0.01$ vs. the E2-treated group. $N=8$, Tukey's test following ANOVA. (C) K252a (200 nM) and BDNFAB (10 μg/ml) significantly inhibited the effect of E2 on the number of presynaptic sites in the mixed neuron culture, whereas ICI (1 μM) did not. *: $p < 0.05$ vs. the control group, #: $p < 0.05$ vs. the E2-treated group. $N=8$, Tukey's test following ANOVA.

slice cultures and subregional neuron cultures were mediated by the common mechanism which is independent of nERs and dependent on endogenous BDNF, suggesting the involvement of BDNF in DG granule cells in the synaptogenic effect of E2 in CA3SL.

2.4. E2 enhanced BDNF release from DG granule cells via nER-independent and PKA-dependent mechanisms

We further examined the association between the effects of E2 and BDNF using subregional hippocampal neuron cultures. The expression levels of BDNF were confirmed for both the Ammon's horn neuron culture and the DG neuron culture by Western blot analysis and enzyme linked immunosorbent assay (ELISA) (Fig. 6). In Western blot analysis, BDNF immunoreactive bands were detected in the control lanes for both cultures, but the OD for the DG neurons was markedly higher than that for the Ammon's horn neurons (Fig. 6A). E2 (1 μM, 24 h) did not affect the expression levels of BNDF in Ammon's horn neurons or DG neurons. ELISA also showed that the

A

B

E2	-	+	+	+	+	+	-	-	-	-
ICI182,780	-	-	+	-	-	-	+	-	-	-
U0126	-	-	-	+	-	-	-	+	-	-
KT5720	-	-	-	-	+	-	-	-	+	-
Rp-cAMP	-	-	-	-	-	+	-	-	-	+

Fig. 7 – Effects of E2 on the BDNF release in the DG neuron culture. (A) Treatment for 10 h with E2 (1 μM) had no effect on the number of presynaptic sites in the DG neuron culture. (B) E2 (1 μM, 10 h) significantly enhanced BDNF release in the DG neuron culture. KT5720 (200 nM) and Rp-cAMP (10 μM) inhibited the effect of E2, whereas ICI (1 μM) and U0126 (10 μM) did not. **: $p<0.01$ vs. the control group, ##: $p<0.01$ vs. the E2-treated group. $N=4$, Tukey's test following ANOVA.
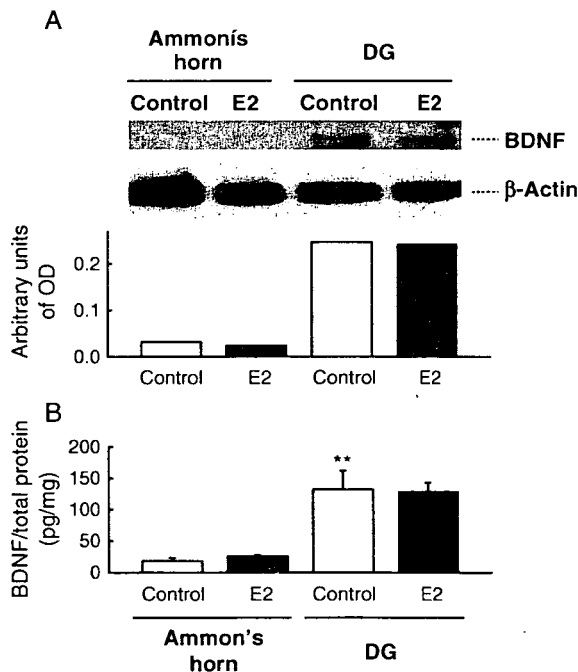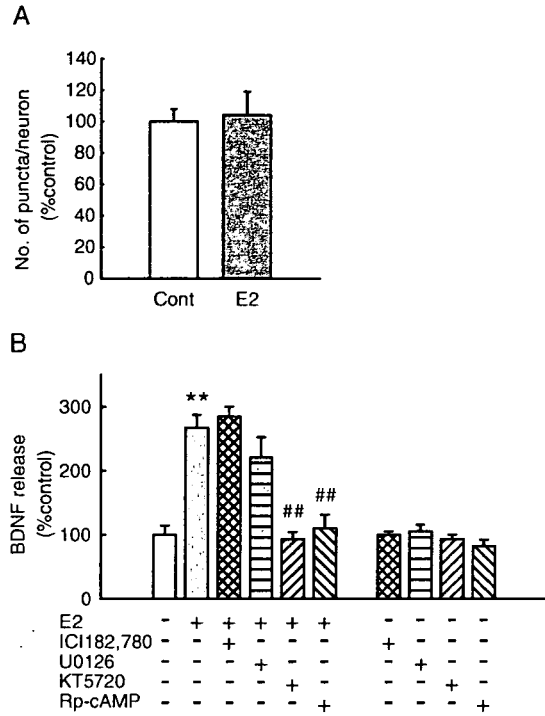
A

Fig. 6 – The expression of BDNF in subregional hippocampal neuron cultures. (A) Western blot analysis of BDNF in subregional hippocampal neuron cultures. The expression level of BDNF of DG neurons was much higher than that of Ammon's horn neurons. E2 (1 μM, 24 h) had no effect on the BDNF expression level. The same results were obtained in 3 independent experiments. (B) ELISA detection of BDNF in subregional hippocampal neuron cultures. The expression level of BDNF in DG neurons was significantly higher than that in Ammon's horn neurons. E2 (1 μM, 24 h) had no effect on the BDNF expression level. **: $p<0.01$ vs. the control group of Ammon's horn neurons. $N=4$, Tukey's test following ANOVA.

expression level of BDNF in DG neurons was remarkably higher than that of Ammon's horn neurons and E2 had no effect on the expression levels in both cultures (Fig. 6B). These results indicate that subregional neuron cultures reflect in vivo pattern of BDNF expression in the hippocampus, in which the highest concentration of BDNF occurs in DG granule cells (Dieni and Rees, 2002; Scharfman et al., 2003). We next examined the possibility that E2 enhances BDNF release from DG granule cells without affecting BDNF expression. The amount of BDNF released into the culture medium of the DG neuron culture was measured by ELISA. We performed ELISA after 10 h of treatment with E2, at the time point when the effect of E2 on the number of presynaptic sites was not yet apparent (Fig. 7A). E2 (1 μM, 10 h) remarkably increased the BDNF release (267 ± 20.5% of control; Fig. 7B). Neither ICI (1 μM) nor U0126 (10 μM) (Ki: 72 nM for MEK1, 58 nM for MEK2) (Duncia et al., 1998), influenced the effect of E2. In contrast, KT5720 (200 nM) (Ki: 56 nM for PKA) (Kase et al., 1987) and Rp-cAMP (10 μM) (Ki: 11 μM for PKA) (Rothermel and Parker Botelho, 1988), suppressed the effect of E2 to the control level. These inhibitors alone had no effects on the basal BDNF release. These results indicate that E2 enhanced BDNF release from DG

granule cells via nER-independent and PKA-dependent mechanisms, which may underlie the effects of E2 described above.

3.   Discussion

In this study, we provided evidence showing that E2 induces synaptogenesis between mossy fibers and CA3 neurons by enhancing BDNF release from DG granule cells in a nER-independent and PKA-dependent manner.

We used subregional hippocampal neuron cultures to investigate the effects of E2 in detail. That these cultures sufficiently maintain their region-specific characters is supported by the following evidence: 1) the morphology of neurons in the Ammon's horn neuron culture was clearly different from that in the DG neuron culture (Fig. 4A). Most cells in the Ammon's horn neuron culture were large and spindle-shaped, which is typical for pyramidal neurons. Most cells in the DG neuron culture were small and granular, which is typical for DG granule cells. 2) DG neurons isolated and cultured using a similar procedure maintain their in vivo physiological properties (Ikegaya et al., 2000). 3) The expression level of BDNF of the cultured DG neurons is much higher than that of the cultured Ammon's horn neurons, reflecting in vivo pattern of BDNF expression in the hippocampus, in which the highest concentration of BDNF occurs in DG granule cells (Dieni and Rees, 2002; Scharfman et al., 2003).

In our study, we prepared hippocampal slices from both genders of P8 rat pups and cultured for 10 days with medium supplemented with horse serum (HS) collected from gelding horses, in which steroid concentrations were under the limits for detection. Because the increases in the expression level of PSD95 and the spine density in CA3 were observed in all slices treated with E2, we consider that the effects of E2 in our study are gender-independent. Currently we are investigating whether or not there is gender difference in the extents of the effects of E2. Organotypic hippocampal slice cultures of P5–9 rat brains are well-established, stable model for investigating hippocampal function including developmental synaptogenesis because neurons maintain synaptogenic ability in each region (CA1, CA3, and DG) (De Simoni et al., 2003; Mizuhashi et al., 2001; Qin et al., 2001). It has been reported that during postnatal development, the capacity of estrogen binding protein is high enough to lower the concentrations of serum estrogens to nonphysiological levels (Germain et al., 1978). This suggests that the conditions for the hippocampal slice culture in the present study more closely represent the postnatal developmental stage. Recently it was clarified that E2 is synthesized from endogenous cholesterol by P45017α and P450 aromatase in hippocampal neurons (Hojo et al., 2004) and that it plays an essential role in the maintenance of synapses (Kretz et al., 2004). The effects of E2 shown here might be achieved by locally synthesized E2 at the postnatal developmental stage. Two previous studies reported the effects of E2 on spinogenesis in cultured hippocampal slices (Kretz et al., 2004; Pozzo-Miller et al., 1999), but their results are conflicting, perhaps because of the effects of various steroids included in the HS in the culture medium.

Our findings suggest that BDNF in DG granule cells mediates the effects of E2. It has been reported that in the hippocampus the highest concentration of BDNF occurs in DG granule cells, especially in their axons, mossy fibers (Dieni and Rees, 2002; Scharfman et al., 2003), from the prenatal period through to adulthood (Dieni and Rees, 2002). The significance of BDNF in DG granule cells, however, had been unknown until Scharfman et al. showed that endogenous BDNF in mossy fibers affected the excitability of CA3 neurons in adult female rats (Scharfman et al., 2003). On the other hand, BDNF has long been known to promote synaptogenesis by maturation of presynaptic sites (Aguado et al., 2003; Seil and Drake-Baumann, 2000). Real-time monitoring revealed that BDNF increases the number of presynaptic sites (Alsina et al., 2001). Presynaptic maturation can induce postsynaptic maturation, as shown by mossy fiber induction of postsynaptic maturation including assembly and clustering of PSD95 on CA3 apical dendrites (Qin et al., 2001). In the present study, BDNF released from DG granule cells may have first increased the number of presynaptic sites by autocrine/paracrine mechanisms, thereby inducing the maturation of postsynaptic sites. In addition to the communication with CA3 pyramidal neurons through giant boutons, mossy fibers also communicate with local circuit interneurons in CA3 through filopodial extensions and en passant boutons (Acsady et al., 1998; Lawrence and McBain, 2003). Although the number of these small terminals is greater than that of giant boutons, we consider that E2 predominantly promoted the synaptogenesis between mossy fibers and CA3 pyramidal neurons in this study because of the following reasons: 1) E2 increased the number of giant boutons, which were identified as mossy fiber terminals containing Zn^{2+} in our previous report (Sato et al., 2002), and 2) the major population of BDNF-positive mossy fiber terminals is those with giant boutons (Danzer and McNamara, 2004). Further experiments using interneuron-specific markers will be necessary to identify the effect of E2 on synaptogenesis between mossy fibers and CA3 interneurons.

E2 enhanced BDNF release from DG granule cells in a nER-independent and PKA-dependent manner. Besides the genomic effects via nERs (ERα and ERβ), recent reports have described the nongenomic effects of estrogens mediated by mERs (Beyer et al., 2003; Kelly and Levin, 2001; Segars and Driggers, 2002). Although the membrane localization of the E2 binding sites is widely accepted, mERs still await isolation and gene cloning. One of the candidate mERs is membrane-localized ERα/β that can activate signal transduction pathways distinct from nERα/β (Razandi et al., 2004; Thomas et al., 2004). Although the mode of action has not been elucidated precisely, ERα has been localized to the neuronal plasma membrane in the hippocampus (Clarke et al., 2000). On the other hand, several reports suggest that the proteins, which are completely different from ERα/β, function as mERs in hypothalamus (Cambiasso and Carrer, 2001), midbrain (Beyer and Karolczak, 2000; Beyer et al., 2002), and neocortex (Toran-Allerand et al., 2002). The effects of E2 observed in our study may have been mediated by one or more mechanisms other than nERs.

It has been reported that E2 modulates the expression of BDNF by genomic (Sohrabji et al., 1995) or nongenomic mechanisms (Ivanova et al., 2001). Unexpectedly, in this

study BDNF expression levels were not affected by E2 (Fig. 6). Instead, E2 enhanced BDNF release from DG granule cells via the activation of the PKA pathway. The PKA/cAMP-responsive element binding protein (CREB) pathway has been shown to lie downstream of mERs in midbrain dopamine neurons (Beyer and Karolczak, 2000; Beyer et al., 2002). The effects of E2 in this study might be mediated by the same type of mERs as those in midbrain dopamine neurons. There are 2 major BDNF secretory pathways (for review, Lessmann et al., 2003): one is the Ca^{2+}-independent constitutive pathway and the other is the Ca^{2+}-dependent regulated pathway. In the regulated pathway, BDNF is sorted to large dense-core vesicles (LDCVs) (Wu et al., 2004) and released in an activity-dependent manner (Haubensak et al., 1998) following slow kinetics typical for protein secretion (Hartmann et al., 2001). BDNF plays an important role in long-term synaptic plasticity (for review, McAllister et al., 1999). BDNF is released selectively by electrical stimulation patterns that induce long-term-potentiation (LTP), thereby modulating the activity-dependent neuronal plasticity (Balkowiec and Katz, 2002; Gartner and Staiger, 2002). cAMP triggers BDNF release in such LTP-inducing condition (Patterson et al., 2001), so E2 might affect synaptic plasticity by way of cAMP-dependent BDNF release.

In ovariectomized adult female rats, E2 enhances the spinogenesis of apical dendrites in CA1 but not in CA3 (Gould et al., 1990). Recent studies have revealed that Akt (protein kinase B) activation via mERs mediates the spinogenesis in CA1 in adult rats (McEwen et al., 2001; Znamensky et al., 2003). On the other hand, there is evidence for another mechanism of E2-induced spinogenesis in embryonic hippocampal neuron cultures. In this system E2 acts via nERs to suppress BDNF expression in γ-aminobutyric acid (GABA) ergic interneurons and to decrease GABAergic inhibition, thereby inducing spinogenesis (Murphy et al., 1998a; Murphy et al., 1998b). It is possible that these mechanisms were also active in our study because E2 increased the spine density in CA1SR in cultured hippocampal slices. But clear differences were observed between the effect in CA1SR and that in CA3SL. The spinogenic effect in CA1SR was much weaker than that in CA3SL (Fig. 2) and the expression of PSD95 in CA1SR was not changed by E2 (Fig. 1). The local assembly of PSD95 is spatially and temporally correlated with the maturation of spine morphogenesis (Okabe et al., 2001: Jontes and Smith, 2000). PSD95 clusters are found in one-half of dendritic filopodia, but in most mature spines (Takahashi et al., 2003). Thus, the spines induced by E2 in CA1SR may be more immature compared with those in CA3SL. The effects of E2 in CA3 through BDNF derived from DG granule cells may be stronger than that in CA1 through the mechanisms described above. The absence of the effect of E2 in CA3 in previous reports (Gould et al., 1990; Znamensky et al., 2003) can be explained if the mechanism that we indicated here is not active in adulthood or the mechanisms demonstrated in the previous reports are active predominantly in CA1.

Our results strongly suggest that E2 induces synaptogenesis between mossy fibers and CA3 neurons by the enhancement of BDNF release from DG granule cells in a nER-

independent and PKA-dependent manner. These data provide evidence that BDNF in DG granule cells has a role in synaptogenesis, and that E2 can modulate this synaptogenic function of BDNF.

---

4. Experimental procedure

4.1. Materials

Millicell-CM was from Millipore (Bedford, MA). Minimal essential medium (MEM), Neurobasal medium (NB) and B-27 supplement were from Gibco Invitrogen Co. (Carlsbad, CA). Donor HS (gelding) was from C-C Biotech Corporation (Valley Center, CA). Paraformaldehyde (PFA), polyoxyethylene (10) octylphenyl ether (Triton X-100), ammonium chloride, dimethylsufoxide (DMSO), L-glutamine, glycine, Tween 20 and sodium azide were from Wako Pure Chemical (Osaka, Japan). K252a was from Calbiochem (Darmstadt, Germany). Anti-BDNF antibodies (AB1534SP and AB1513P) and Chemikine BDNF Sandwich ELISA kit were from Chemicon (Temecula, CA). ICI was from Tocris (Ballwin, MO). Mouse monoclonal immunoglobulin G (IgG) to PSD95 (K28/43) was from Upstate Biotechnology (Lake Placid, NY). Alexa Fluor 488 rabbit anti-mouse IgG, NeuroTrace fluorescent Nissl, DiI and FM1-43 were from Molecular Probes (Eugene, OR). E2, poly-L-lysine, cytosine β-D-arabino-furanoside (AraC), ethylenediaminetetraacetic acid (EDTA), phenylmethyl-sulphonyl fluoride, leupeptin, antipain hydrochloride, aprotinin, Trizma hydrochloride, bovine serum albumin (BSA), rabbit polyclonal IgG to β-actin, peroxidase-conjugated anti-rabbit IgG, tetrodotoxin (TTX), KT5720, and Rp-cAMP were from Sigma (St. Louis, MO). U0126 was from Promega (Madison, WI). Sodium dodecyl sulphate (SDS) was from Nacalai tesque (Kyoto, Japan). ADVASEP-7 was from Biotium (Hayward, CA). Enhanced chemiluminescence (ECL) plus Western blotting detection kit was from Amersham Biosciences (Arlington Heights, IL). Fluorescent images were obtained using a BioRad μ-Radiance laser scanning confocal system (Hercules, CA) attached to Nikon inverted microscope (Tokyo, Japan). Image analysis was performed using Adobe Photoshop 7.0 (Mountain View, CA).

4.2. Organotypic hippocampal slice culture

All animal procedures were in accordance with the guidelines of the National Institute of Health Sciences, Japan, to minimize pain or discomfort. Organotypic slice cultures of both genders of P8 Wistar rat hippocampi were prepared according to the method of Sato et al. (2002). Briefly, horizontal medial hippocampal slices (300-μm thick) were placed on Millicell-CM transmembranes and cultured with 0.7 ml of the culture media (50% [vol/vol] MEM, 25% [vol/vol] Hank's balanced salt solution [HBSS], and 25% [vol/vol] HS [gelding] supplemented with 6.5 mg/ml glucose, 50 U/ml penicillin G potassium and 100 μg/ml streptomycin sulphate). All experiments were performed at 10 days in vitro (DIV) because cultured hippocampal slices recover from damage by sectioning and complete the trisynaptic neuronal circuitry (DG→CA3→CA1) at 10-14 DIV (Nakagami et al., 1997).

4.3.   Immunohistochemistry

Immunostaining of cultured hippocampal slices was performed according to the method of Qin et al. (2001) with modifications. Slices were fixed with ice-cold 4% (wt/vol) PFA in 0.1 M phosphate buffer (PB) for 10 min at 4 °C, washed with phosphate buffered saline (PBS) (5 min×3), and treated with 1% (vol/vol) Triton X-100 in PBS overnight at 4 °C. Slices were then blocked with 50 mM ammonium chloride for 30 min at 4 °C and 20% HS in PBS for 30 min at 4 °C. Subsequent steps were carried out using PBS containing 1% HS. Slices were treated with mouse monoclonal IgG to PSD95 (1:1000) overnight at 4 °C, washed (15 min×3), and treated with Alexa Fluor 488 rabbit anti-mouse IgG (1:1000) overnight at 4 °C. After washing (15 min×3), fluorescent images were obtained by confocal microscopy (BioRad μ-Radiance laser scanning confocal system) using a 4×objective. Black level was set so that the averaged fluorescence intensity of 5 independent squares (20 μm×20 μm) placed at the medial position of CA1 stratum pyramidale (SP) of the control slice had the same value as that of the outside of the slice. Gain level was set so that the averaged fluorescence intensity of 5 squares (20 μm×20 μm) placed at the medial position of CA3SL of the control slice was at the half-maximum level. In gray-scale mode under these settings, the major synaptic sites appeared as fluorescent compartments as shown in Fig. 1B. When we outlined these compartments as indicated in Fig. 1B and calculated the areas, the values were constant regardless of the treatment (data not shown), so, we measured the averaged fluorescence intensity of each compartment (an outlined area) and subtracted the background intensity to quantify the expression level of PSD95 of each synaptic site. Because slices were cultured after removing entorhinal cortex, we quantified the expression of PSD95 in CA1SR, CA1SO, CA3SL, and CA3SO, the synaptic sites which maintain the intact presynaptic and postsynaptic cells (Fig. 1B).

4.4.   DiI staining

Cultured hippocampal slices were fixed with 4% PFA for 30 min at 4 °C. The fixative above the transmembrane was removed and DiI crystals were embedded into CA1SO and CA3SO under the light microscope. After 3 days of incubation at 4 °C, fluorescent images were obtained by confocal microscopy using a 60×objective. Horizontal optical sections were taken at 0.5 μm steps and the resultant z-series images were summed into a flat image. Spines (both dendritic filopodia and mature spines) were counted at the proximal sites of apical dendrites projecting from pyramidal cell bodies. For double labeling with DiI and PSD95 immunostaining, slices were immunostained after 3 days of incubation with DiI crystals.

4.5.   Fluorescent Nissl staining

Cultured hippocampal slices were fixed with 4% PFA for 60 min at 4 °C. Subsequent steps were carried out at room temperature. After washing with PBS (15 min×3), the slices were treated with 0.1% Triton X-100 in PBS for 60 min, washed with PBS for 10 min, and incubated with NeuroTrace fluorescent Nissl (1:30 in PBS) for 40 min in a dark room. The incubation was terminated by a 10 min wash with 0.1% Triton X-100 in PBS, followed by 2 h wash with PBS. Fluorescent images were obtained by confocal microscopy using a 60×objective.

4.6.   Subregional hippocampal neuron culture

Subregional neuron cultures of both genders of P3 Wistar rat hippocampi were prepared according to the method of Ikegaya et al. (2000). Ammon's horn and DG were isolated from hippocampi with extreme care so as not to mix these 2 regions (Fig. 4A, right). Dissociated cells from Ammon's horn, DG, or a combination of these regions were suspended in a 1:1 mixture of astrocyte-conditioned medium (ACM) and NB/B27 medium (2% [v/v] B-27 supplement and 73 μg/ml L-glutamine in NB) and plated onto 48-well plates coated with poly-L-lysine. After 24 h, the medium was changed to ACM-free NB/B-27 medium containing 2 μM AraC. Cells derived from each region were cultured for 7 days at the same cell density (2×10^4 cells/cm^2 for FM1-43 analysis, 5×10^5 cells/cm^2 for Western blot analysis and ELISA detection of BDNF). All surviving cells were immunohistochemically confirmed to be neurons using anti-NeuN antibody (data not shown).

4.7.   FM1-43 analysis

After 1 h of incubation with HBSS at 37 °C, cultured neurons were treated with 10 μM FM1-43, a styryl pyridinium dye (Cochilla et al., 1999) in high K$^+$-HBSS (20 mM KCl; osmolarity maintained by concomitant decrease in sodium concentration) for 2 min and washed gently with HBSS for 1 min. To reduce background staining, neurons were washed with 20 μM ADVASEP-7, a sulphobutylated derivative of β-cyclodextrin (Tait et al., 1992) for 1 min. ADVASEP-7 has a higher affinity for FM1-43 than plasma membranes and has been shown to greatly reduce background staining in brain slices (Kay et al., 1999). After the incubation with 10 μM TTX for 30 min, three images ([1] stained image; [2] destained image obtained after the treatment with high K$^+$-HBSS; and [3] differential interference contrast [DIC] image) were obtained for each microscopic field of view using confocal microscopy with a 10× objective. The second image was subtracted from the first, which revealed the presynaptic sites where depolarization-specific release had occurred (Fig. 4C, top panels). The fluorescent puncta in each microscopic field of view were counted. The number of synapses per neuron was estimated by dividing the total number of puncta by the number of neurons observed in the third (DIC) image (Fig. 4C, bottom panels).

4.8.   Western blot analysis

Cultured neurons were washed twice with ice-cold PBS and then harvested on ice with 50 mM Tris buffer (pH 7.2) containing 1 mM EDTA, 1 mM phenylmethylsulphonyl fluoride, 1 mM leupeptin, 1 μg/ml antipain and 1 μg/ml aprotinin. After intense sonication (23 kHz, 1 min×3), the cell suspension was centrifuged at 800×g for 5 min at 4 °C. An

aliquot of this supernatant was removed for the protein assay. Another aliquot was diluted in SDS sample buffer. Protein samples containing an equal amount of protein were separated by electrophoresis on 10% polyacrylamide-SDS gels and transferred onto polyvinyliden difluoride membranes in 49.6 mM Tris, 384 mM glycine and 0.01% (wt/vol) SDS at 30 V overnight followed by 80 V for 1 h. The membranes were incubated with Tris-buffered saline (TBS) containing 0.1% (vol/vol) Tween 20, 5% (wt/vol) skim milk, 2% (wt/vol) BSA, and 0.1% (wt/vol) sodium azide for 1 h, followed by overnight incubation with protein A purified rabbit anti-BDNF polyclonal antibody (AB1534SP, Chemicon) (1:1000) or rabbit polyclonal IgG to β-actin (1:1000) at 4 °C. After washing (30 min), the membranes were then incubated with peroxidase-conjugated anti-rabbit IgG (1:1000) for 1 h at room temperature. Immunoreactive bands were visualized using the ECL kit. Optical densities (ODs) of immunoreactive bands were measured based on a gray scale of 0–256 arbitrary units. Background was subtracted from the OD and this corrected value was normalized to the corrected value of the β-actin band obtained from the same sample.

4.9. ELISA detection of BDNF

In comparison of BDNF contents in cultured DG neurons and cultured Ammon's horn neurons, cells were washed twice with ice-cold PBS and then harvested on ice with homogenization buffer consisting of 100 mM Trin/HCl (pH7), containing 2% (wt/vol) BSA, 1 M NaCl, 4 mM EDTA.Na2, 2% (vol/vol) Triton X-100, 0.1% (wt/vol) sodium azide, 5 μg/ml aprotinin, 0.5 μg/ml antipain, 157 μg/ml benzamidine, 0.1 μg/ml pepstatin A and 17 μg/ml phenylmethyl–sulphonyl fluoride. After intense sonication (23 kHz, 1 min×3), the homogenates are centrifuged at 14,000×g for 30 min. An aliquot of this supernatant was removed for the protein assay. Another aliquot was subjected to the calculation of BDNF concentration by the Chemikine BDNF sandwich ELISA kit. The plates, which were pre-coated with monoclonal antibodies against BDNF, were incubated with 100 μl of supernatant in each well overnight, followed by incubation with the secondary antibody for 3 h and color developing procedures for 1 h. Immediately after the stop solution included in the kit was added, the ODs of 450 nm were measured. A standard curve was run for each plate and linearity was confirmed for all detections. Because the lower detection limit of the kit is 7.8 pg/ml, we used data from the experiments in which the control value was higher than this limit. The concentration of BDNF was normalized to the total amount of protein. In the calculation of BDNF contents in the culture media, the culture media were collected after 10 h of incubation with E2, centrifuged at 1500×g, and the concentration of BDNF in the supernatants was determined by ELISA. Because in this case the values of the control group varied from experiment to experiment by several folds, we set 'basal value' in each experiment. 24 h after medium change, BDNF concentrations in the culture media were calculated and averaged for 4 wells in one experiment. This value was taken as the 'basal value' and the data were normalized to this 'basal value' in each experiment.

4.10. Drug treatment

E2 was dissolved at 100 mM in ethanol and diluted to the final concentrations with the culture medium. For PSD95 immunohistochemistry and FM1-43 analysis, cultured slices and cells were treated with various concentrations of E2 for 24 h. ICI (Ki: 1.5 nM for ERα, 6.4 nM for ERβ; Kuiper et al., 1997) was dissolved at 1 mM in ethanol and co-applied at 1 μM with E2. K252a (Squinto et al., 1991; Bothwell, 1995) was dissolved at 1 mM in DMSO and co-applied at 200 nM with E2. This concentration completely blocks the effect of BDNF in cultured hippocampal slices (Koyama et al., 2004). BDNFAB (protein A purified sheep anti-BDNF polyclonal antibody, AB1513SP, Chemicon) was dissolved in the culture medium at 10 μg/ml. This concentration blocks the effect of endogenous BDNF (Rasika et al., 1999; Matsunaga et al., 2004). For ELISA detection of the released BDNF, cultured cells were treated with E2 for 10 h. KT5720 (Ki: 56 nM) (Kase et al., 1987) was dissolved in the ethanol at 1 mM and co-applied at 200 nM with E2. Rp-cAMP (Ki: 11 μM) (Rothermel and Parker Botelho, 1988) was dissolved in PBS at 10 mM and co-applied at 10 μM with E2. U0126 (Ki: 72 nM for MEK1, 58 nM for MEK2) (Duncia et al., 1998) was dissolved in DMSO at 10 mM and co-applied at 10 μM with E2. We also confirmed beforehand that 0.1% ethanol or 0.1% DMSO (the maximal concentration used for vehicle in our experiments) alone had no effects in cultured hippocampal slices and subregional hippocampal neuron cultures (Fig. S1).

4.11. Data analysis

All data regarding the expression level of PSD95, the spine density, and the number of FM1-43 positive puncta, were quantified in a blinded manner. For quantification of PSD-95 signals, the fluorescence intensities in the synaptic sites were averaged for 4 slices in one experiment. These values were then averaged for 8 independent experiments (separate platings) and statistical analysis was performed using one-way repeated-measure analysis of variance (ANOVA) and the post hoc Tukey's test for multiple pairwise comparisons. Data are shown as the values normalized to that of CA1SR in the control group. The spine densities (the number of spines per μm of dendrite) averaged for 8 to 10 neurons per slice were averaged for 4 slices in 1 experiment. These values were then averaged for 8 independent experiments (separate platings) and statistical analysis was performed using the Student's t test. For FM1-43 analysis, the numbers of presynaptic sites (per neuron) were averaged for 4 wells in 1 experiment. These values were then averaged for 8 independent experiments (separate platings) and statistical analysis was performed using the Student's t test. In multiple pharmacological treatments, data were collected according to the methods described above, and statistical analysis was performed by one-way repeated-measure ANOVA and the post hoc Tukey's test for multiple pairwise comparisons. Data were shown as the values normalized to that of the control group. For ELISA detection of BDNF expression, the normalized values (BDNF/ total protein) were averaged for 4 wells in one experiment. These values were then averaged for 4 independent experiments (separate platings) and statistical analysis was